Wesleyan University

Heat Transport in $\mathcal{PT}$-Symmetric Harmonic Chains

by

Mei Chai Zheng

Faculty Advisor: Dr. Tsampikos Kottos

A Dissertation submitted to the
faculty of Wesleyan University
in partial fulfillment of the requirements for the
Degree of Master of Arts

Middletown, Connecticut May, 2011

Abstract

This thesis explores heat transport in harmonic chains with active elements where delicately balanced attenuation and amplification of energy is imposed. Using the mathematical tools developed in the framework of statistical mechanics and stochastic processes, we are able to quantify the non-equilibrium steady state properties (such as the heat flux) of these systems. We show that they exhibit unique heat transport properties when coupled to two thermal baths of different temperatures. Specifically, our study reveals that the heat flux has a negative differential thermal conductance that is independent of the bath temperatures at the chain ends, and shows non-reciprocal heat flow with respect to the two baths. We propose an electronic set-up that is capable of demonstrating the novel qualitative features of our thermal chain. Our results may pave the way toward new technologies in engineering thermal devices as well as a better microscopic understanding of heat transport.

Dedication

给爸爸妈妈

千言万语尽在不言中

Acknowledgments

I am very grateful for another year at Wesleyan. I would like to thank everyone and everything that made this year a success.

First, I would like to thank my advisor, Tsampikos Kottos, who dedicated an ample amount of time helping me improve my research and scientific communication skills. Thank you for your encouragement in my pursuit of science!

Next, I want to thank the faculty of the Wesleyan Physics Department and the members of my research group (WTICS). I would also like to thank all of my collaborators for insightful discussions. A big Vielen Dank is due to Ragnar for his friendship and his patience during the technical difficulties during our skype conference meetings. I also owe MPI a Thanks for their hospitality during my summers there. I would like to acknowledge all of the funding that made my research work possible the Wesleyan BA/MA program and DFG Research Unit 760.

I want to thank Wesleyan Reslife, my fellow RA's, as well as my residents. Fulfilling program requirements allowed me to take a break from physics and laugh while we painted bricks, went apple picking and attended social justice events.

I am thankful for friends, who kept me sane during the stressful periods of GRE, grad school applications, classes, research and thesis writing! Honorable mentions are due to Hamid, Neda, Roy, Nam, Amanda, and Lesley. Thanks for making me laugh, for

getting me away from my desk, and for all of your love and care.

I am indebted to my family. I would like to thank my mom and dad for their understanding and their support in my studies. I especially want to thank my mom for her positive attitude and her comfort that kept me going when I was under the pressure of deadlines. I also want to thank my siblings especially my older brother for taking care of my other duties, such as filing my taxes.

Last but not least, I thank God for carrying me through yet another year.

Contents

1 Introduction **1**

2 $\mathcal{PT}$-Symmetry **3**

2.1 Introduction to $\mathcal{PT}$-symmetry 4

2.1.1 The two level system: Eigenvalue and Eigenvector Analysis . . . 5

2.1.2 The two level system: Dynamics 8

2.2 Applications of $\mathcal{PT}$-Symmetry 9

2.2.1 Observations of $\mathcal{PT}$-dynamics in Photorefractive structures . . . 11

2.2.2 Unidirectional nonlinear $\mathcal{PT}$-symmetric optical structures 12

2.3 Summary 14

3 Basic Models and Theory of Heat Transport **15**

3.1 Definitions 16

3.1.1 Models 16

3.1.2 Temperature 19

3.1.3 Flux 19

3.2 Deterministic Bath 21

3.3 Stochastic Bath 23

3.4 Summary 26

4 Transport in $\mathcal{PT}$-Symmetric Harmonic Chains **27**

4.1 Model and Mathematical Formalism 28
4.1.1 Mathematical Formalism for $\kappa = 0$ 29
4.1.2 Mathematical Formalism for $\kappa \neq 0$ 30
4.1.3 Dimer example 32
4.2 Beyond the Dimer 37
4.2.1 Spectra Analysis 38
4.2.2 Analysis of dynamical properties 38
4.3 Electronic Implementation 42
4.4 Summary 43

5 Conclusion **44**

A Eigenvalues in the Broken $\mathcal{PT}$ Phase **46**

B Left and Right Eigenvectors **48**

C A Rigorous Definition of Temperature **49**

D Nosè-Hoover Thermostat **51**

E Algebra for the correlation function **55**

F Implementing Ito Calculus **57**

G Fokker-Planck Equation **59**

List of Figures

2.1 Eigenvalues of the simple $\mathcal{PT}$-symmetric system 6
2.2 Eigenvectors of the $\mathcal{PT}$-symmetric Hamiltonian 7
2.3 Numerical stimulation of of light beam propagation the active "$\mathcal{PT}$-symmetric system". 10
2.4 Experimental set-up of the active $\mathcal{PT}$-symmetric dimer. 11
2.5 Experimental Results of the active "$\mathcal{PT}$-symmetric system" 12
2.6 Beam propagation in two coupled nonlinear waveguides 13

3.1 A schematic figure of a chain of $N = 8$ coupled oscillators 17

4.1 Schematic illustration of an active harmonic chain model 29
4.2 The real and imaginary part of the eigenfrequencies Vs. the amplification/attenuation parameter,γ. 30
4.3 A schematic illustration of an active harmonic dimer model: $N = 2$. . . 33
4.4 The real and imaginary part of the eigenfrequencies Vs. the amplification/attenuation parameter for the "closed "dimer. 34
4.5 The real and imaginary part of the eigenfrequencies Vs. the amplification/attenuation parameter for the "open "dimer. 35
4.6 λ Vs. γ with different Δ for the dimer 36
4.7 The spectra of the $\mathcal{PT}$-symmetric harmonic chain of Fig. 4.1 39
4.8 Heat flux as a function of γ for various temperatures 40

4.9 Flux and temperature profiles for two different situations of a chain with $N_a = 8$ and $N_b = 50$ sites 42
4.10 Electronic implementation of a simplified $N_a = 2$ (dimer) chain. 43

Chapter 1

Introduction

The study of heat transport and the investigation of new schemes for its control is one of the main challenges of statistical physics and thermal engineering. From a fundamental point of view, the question is to understand macroscopic phenomena and their statistical properties in terms of deterministic microscopic dynamics and, in particular, to connect macroscopic irreversibility with time reversible microscopic evolution of a system of interacting particles. On the technological side, there is pressure to engineer high efficiency thermoelectric materials and design efficient schemes for the control of heat transport. As a result, the study of heat transport in low dimensional systems such as atom chains or various nanostructures, has produced many exciting ideas [1–3] ranging from heat rectification [4, 5] to heat logic gates [6]. In fact, some of these exciting theoretical suggestions have recently been experimentally realized [7, 8]. Despite all this activity, our understanding of heat transport is far from being settled. For example, it is still not understood exactly what are the sufficient and necessary conditions in terms of microscopic dynamics for the validity of Fourier's law of heat conduction [9]. Even in linear (harmonic) oscillator chains, energy transport can have various different features, depending on the (mass) disorder or spectral properties of the heat baths [3].

In contrast to the traditional conservative systems employed in the study of heat trans-

port, this thesis studies a class of systems that incorporate both attenuation and amplification in a balanced manner. Their main characteristic is that they respect the combined Parity ($\mathcal{P}$) and Time-Reversal ($\mathcal{T}$) symmetry without being Parity or Time symmetric separately. This thesis will introduce $\mathcal{PT}$-symmetry in the framework of heat transport. The main results of this study have been submitted for publication [10].

The structure of this thesis is as follow:

- In Chapter 2, we will introduce the concept of $\mathcal{PT}$-symmetry in the general framework of quantum mechanics and demonstrate the main features using a simple, realistic model. We will conclude with the presentation of some applications to systems in the optics framework [11–14].
- In Chapter 3, we will present the basic models and the theoretical grounds on which heat transport is studied. The concepts of temperature, flux, and thermal reservoirs will be discussed.
- Chapter 4 introduces the $\mathcal{PT}$-symmetric harmonic chain and its mathematical description. The spectral and non-equilibrium steady state properties will also be discussed. The final goal is to obtain a theoretical description of the heat flux.
- In Chapter 5, we will conclude with the main points of the thesis and provide some future outlook.

Chapter 2

$\mathcal{PT}$-Symmetry

In order for a quantum theory to describe physical systems, it must (i) have an energy spectrum that is real and bounded from below, (ii) possess a Hilbert space of state vectors whose inner products have a positive norm, and (iii) have unitary time evolution [15]. These conditions are all satisfied by a Hermitian Hamiltonian, $H = H^\dagger$. However, it has been found that not only Hermitian Hamiltonians satisfy these conditions. Specifically, it has been shown that a $\mathcal{PT}$-symmetric Hamiltonian H (*i.e.* H commutes with the combine Parity ($\mathcal{P}$) and Time ($\mathcal{T}$) operator) can respect all the constrains that make a quantum theory viable. This notion of $\mathcal{PT}$-symmetry was first introduced by C. M. Bender and has now been studied in many different fields of physics ranging from quantum field theory and mathematical physics [15–18] to solid-state physics [19] and linear [11, 20, 21] and nonlinear [22] optics.

This chapter will introduce the notions of the $\mathcal{P}$ and $\mathcal{T}$ operators in the general framework of quantum mechanics in section 2.1. Within that section, we will discuss the properties of the eigenvalues and eigenvectors of the simplest $\mathcal{PT}$-symmetric system, a two-level system in section 2.1.1. Its dynamical properties will be analyzed in section 2.1.2. Next, we will discuss the application of $\mathcal{PT}$-symmetry in optics and present an experimental realization of the two-level system in section 2.2.1. We will also present

a theoretical result of this system with nonlinearity in section 2.2.2. Lastly, we will summarize in section 2.3. Most of the discussion in this chapter is taken from Ref. [23].

2.1 Introduction to $\mathcal{PT}$-symmetry

Parity ($\mathcal{P}$) and time-reversal ($\mathcal{T}$) symmetries are fundamental notions in physics. $\mathcal{P}$ is a linear operator that performs a spatial reflection: $\hat{x} \to -\hat{x}$ and $\hat{p} \to -\hat{p}$, where $\hat{x}$ and $\hat{p}$ are the position and the momentum operator, respectively. The operator $\mathcal{T}$ is an anti-linear operator that performs a complex conjugation: $\hat{x} \to \hat{x}$, $\hat{p} \to -\hat{p}$ and $i \to -i$. There has been a rising interest in systems that do not obey the individual $\mathcal{P}$ and $\mathcal{T}$ symmetries but which respect the combined $\mathcal{PT}$ symmetry [12]. Such systems are described by a Hamiltonian (H) that commutes with the combined $\mathcal{PT}$ operator, *i.e.* $[\mathcal{PT}, H] = 0$. Despite the fact that $\mathcal{PT}$-Hamiltonians can, in general, be non-Hermitian, their spectra can be entirely real. Therefore, such Hamiltonians can physically model phenomenologically open systems. The departure from Hermiticity is due to the presence of various gain/loss mechanisms which occur in a balanced manner, so that the net loss or gain of "particles" is zero. Furthermore, as some gain/loss parameter γ that controls the degree of non-Hermiticity of H gets a critical value $\gamma_{\mathcal{PT}}$, a spontaneous $\mathcal{PT}$ symmetry breaking can occur. For $\gamma > \gamma_{\mathcal{PT}}$, the eigenfunctions of H cease to be eigenfunctions of the $\mathcal{PT}$-operator, despite the fact that H and the $\mathcal{PT}$-operator commute [15]. This happens because the $\mathcal{PT}$-operator is anti-linear, and thus the eigenstates of H may or may not be eigenstates of $\mathcal{PT}$. As a consequence, in the *broken $\mathcal{PT}$-symmetric phase*, the spectrum becomes partially or completely complex. The other limiting case, where both H and $\mathcal{PT}$ share the same set of eigenvectors, corresponds to the so-called *exact $\mathcal{PT}$-symmetric phase*, in which the spectrum is real (see Appendix C of [23]). The simplest physical model showing $\mathcal{PT}$-symmetric properties is the two level system. In the next section, we will refer to the physical realizations of this model. We will analyze its spectra, eigenfunction and dynamical properties. Due to its extraordinary simplicity it

offers an educational paradigm to understand the basic ideas of $\mathcal{PT}$-symmetry.

2.1.1 The two level system: Eigenvalue and Eigenvector Analysis

One can show (see Appendix D of Ref. [23]) that $\mathcal{PT}$-symmetry requires the real part of the potential to be an even function of position; whereas the imaginary part is an odd function. The simplest possible $\mathcal{PT}$-Hamiltonian is illustrated by the following matrix

$$H = \begin{pmatrix} v_0 + i\gamma & \kappa \\ \kappa & v_0 - i\gamma \end{pmatrix} \tag{2.1}$$

where the parameters v_0, γ and κ are real and correspond to the real, and imaginary part of the potential, and the coupling strength between two energy levels, respectively. It is obvious that this Hamiltonian is not Hermitian, but one can easily verify that it is $\mathcal{PT}$ -symmetric, where the parity operator, $\mathcal{P}$, is simply the Pauli matrix, σ_x, and $\mathcal{T}$ performs the complex conjugation.

The eigenvalues of this Hamiltonian can be found via a diagonalization to be

$$E_n = \varepsilon_n + i\Gamma_n = \pm\sqrt{\kappa^2 - \gamma^2} \tag{2.2}$$

where $n = 1, 2$ corresponds to the two $(+, -)$ levels. From the above equation, it is clear that there are two parametric regimes for this Hamiltonian. When $\gamma^2 < \kappa^2$, the energy eigenvalues are real (see Appendix C of Ref. [23]). On the other hand, for $\gamma^2 > \kappa^2$, the eigenvalues form a complex-conjugate pair (see Appendix A). The sharp transition from a real to a complex spectrum that take place at $\gamma_{\mathcal{PT}} = \kappa$, is coined *spontaneous $\mathcal{PT}$-symmetry breaking*. These eigenvalues, for $\kappa = 1$, are plotted as a function of γ in Fig. 2.1.

The corresponding normalized eigenvectors take the following form:

$$|E_1\rangle = \frac{1}{\sqrt{2\cos\alpha}} \begin{pmatrix} e^{i\frac{\alpha}{2}} \\ e^{-i\frac{\alpha}{2}} \end{pmatrix}; \qquad |E_2\rangle = \frac{1}{\sqrt{2\cos\alpha}} \begin{pmatrix} ie^{-i\frac{\alpha}{2}} \\ -ie^{i\frac{\alpha}{2}} \end{pmatrix} \tag{2.3}$$

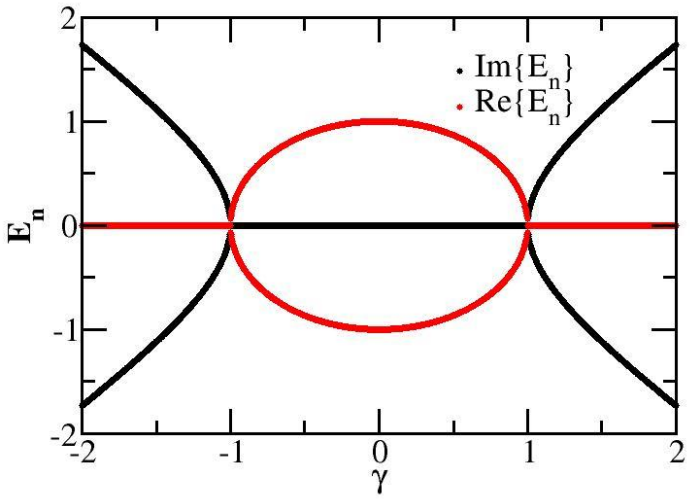

Figure 2.1: Eigenvalues of the simple $\mathcal{PT}$-symmetric system, described by the matrix model (2.1), as a function of γ. This corresponds to Eq.(2.2) for $\kappa = 1$. The red corresponds to ε_n while the black corresponds to Γ_n. For $\gamma > \gamma_{\mathcal{PT}}$, we enter the broken $\mathcal{PT}$-phase and the branching of the imaginary part is characterized by the square root behavior of Eq. (2.2).

where $\sin(\alpha) = \frac{\gamma}{\kappa}$. Let us consider these eigenvectors for the cases above and below the phase transition point, $\gamma_{\mathcal{PT}} = \kappa$. Below this point, $\sin(\alpha) < 1$, giving $\alpha \in \Re$. In this case, we see that these eigenvectors are also the eigenvectors of the $\mathcal{PT}$ operator. The norm, $I = |\psi|^2$, of these two eigenfunctions coincide and is spatially symmetric as shown by the violet color in Fig. 2.2. On the other hand, above the phase transition point, $\sin(\alpha) > 1$, *i.e.* $\alpha \in \Im$. In this case, they are no longer spatially symmetric as shown by the blue and orange color in Fig. 2.2 and are not any more eigenfunctions of the $\mathcal{PT}$ -operator.

In fact, for the non-Hermitian Hamiltonian discussed above, the eigenvectors are bi-orthogonal, *i.e.* the left and right eigenvectors ($\langle L_n|$ and $|R_n\rangle$ respectively), defined as

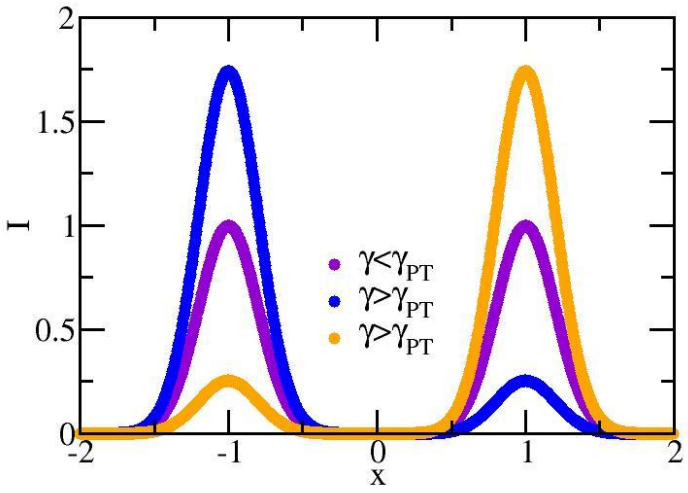

Figure 2.2: $I = |\psi_{1,2}|^2$ of a $\mathcal{PT}$-symmetric system for $\gamma < \gamma_{\mathcal{PT}}$ and $\gamma > \gamma_{\mathcal{PT}}$ when $\kappa = 1$. The violet corresponds to $|\psi_{1,2}|^2$ for $\gamma < \gamma_{\mathcal{PT}}$. The blue and the orange correspond to $|\psi_{1,2}|^2$ for $\gamma < \gamma_{\mathcal{PT}}$.

$\langle L_n|H = \langle L_n|E_n$ and $H|R_n\rangle = E_n|R_n\rangle$, are distinct and $\langle L_n| \neq |R_n\rangle^\dagger$. Therefore, they do not respect the standard (Euclidian) ortho-normalization condition. Previously, we have only referred to the right eigenvectors, namely $|E_n\rangle = |R_n\rangle$. It can be shown however, that in the case of $\mathcal{PT}$-symmetric matrices, the left eigenvector is equal to the transpose of the corresponding right one (see Appendix B). The normalization constant $\frac{1}{\sqrt{2\cos\alpha}}$ is found via the following normalization condition

$$\langle L_n|R_m\rangle = \delta_{nm}, \tag{2.4}$$

with the following completeness relation,

$$\sum_n |R_n\rangle \langle L_n| = 1. \tag{2.5}$$

2.1.2 The two level system: Dynamics

The time evolution of a wavefunction $\psi(t) = (a(t), b(t))^T$, that is generated by the $\mathcal{PT}$-Hamiltonian H of Eq. (2.1) is given by the following set of coupled differential equations:

$$\begin{aligned} i\frac{da(t)}{dt} &= +i\gamma a(t) + \kappa b(t) \\ i\frac{db(t)}{dt} &= -i\gamma b(t) + \kappa a(t) \end{aligned} \tag{2.6}$$

where $a(t)$ and $b(t)$ correspond to the components of the modes and t is the time. The resulting dynamics can be understood by considering its corresponding Hamiltonian (2.1) in terms of the *Pauli Matrix* [24]:

$$H = \omega\hat{\sigma}\hat{n} \tag{2.7}$$

in which $\omega = \sqrt{k^2 - \gamma^2}$ is half of the energy difference, $\hat{\sigma}$ is a vector that consisted of Pauli matrices and $\hat{n} = \left(\frac{1}{\omega}\right)(\kappa, 0, i\gamma)$ is a unit vector. Using the matrix identity

$$\hat{U} = \exp(-iHt) = \cos(\omega t)\hat{1} - i\sin(\omega t)\hat{\sigma}\hat{n} \tag{2.8}$$

where, $\hat{1}$ is the unit matrix, a generic initial state evolving under the non-Hermitian Hamiltonian, Eq. (2.7), takes the following form

$$|\psi(t)\rangle = \hat{U}\left\{c_1|\psi_1\rangle + c_2|\psi_2\rangle\right\} = \frac{1}{\cos\alpha}\begin{pmatrix} c_1\cos\left(\frac{\omega t}{2} - \alpha\right) - c_2 i\sin\left(\frac{\omega t}{2}\right) \\ c_2\cos\left(\frac{\omega t}{2} + \alpha\right) - c_1 i\sin\left(\frac{\omega t}{2}\right) \end{pmatrix}, \tag{2.9}$$

where $\psi_1 = \begin{pmatrix} 1 \\ 0 \end{pmatrix}$ and $\psi_2 = \begin{pmatrix} 0 \\ 1 \end{pmatrix}$ and c_1, c_2 are some generic coefficients that respect the normalization.

The total norm, $I(t) = |\psi(t)|^2$, yields

$$I(t) = \frac{1}{2\cos^2\alpha}\left(\cos^2\left(\frac{\omega t}{2} - \alpha\right) + 2\sin^2\left(\frac{\omega t}{2}\right) + \cos^2\left(\frac{\omega t}{2} + \alpha\right)\right) \tag{2.10}$$

From the above expression, $I(t) = 1$ for $\gamma = 0$ *i.e.* we have norm conservation as shown in Fig. 2.3a. In addition, in this (Hermitian) case, a reciprocal norm dynamics is

observed, *i.e.* the dynamics starting at one energy level mirrors the dynamics starting at the other energy level. However, once the system starts to deviate from Hermiticity (*i.e.* $\gamma \neq 0$), the total norm starts to deviate from 1. In fact, from Eq. (2.10) for the $\gamma < \kappa$ case, we deduce that, the norm, I, oscillates as the square of sinusoidal functions. At the same time, the norm evolution is not any more reciprocal with respect to the axis of symmetry of the two level system *i.e.* the output state depends strongly on which energy level we have initially excited. This non-reciprocal dynamics is a novel characteristic of $\mathcal{PT}$-systems and can be of extreme importance for technological applications (like integrated optical diodes etc.). Nevertheless, one can prove that in this regime of $\gamma < \kappa$, the total norm is bounded. For $\gamma > \kappa$, we enter the broken $\mathcal{PT}$-symmetric phase. In this case, $\omega \in \Im$ and $\alpha \in \Im$; thereby making the total norm behave as hyperbolic functions. In other words, the total norm grows exponentially as seen in Fig. 2.3c. Also in this case, the norm-dynamics is non-reciprocal. What happens at the spontaneous $\mathcal{PT}$-symmetry breaking point? Let us recall that the spontaneous $\mathcal{PT}$-symmetry breaking point, $\gamma_{\mathcal{PT}}$, occurs when $\gamma = \kappa$. At this transition point, $\omega = 0$ and $\alpha = \frac{\pi}{2}$. Plugging these values into Eq. (2.10) yields an indeterminate form of $\frac{0^2}{0^2}$. Applying L'Hôspital's Rule twice to Eq. (2.10) yields the result for the total norm at the transition point: $I(t) \sim t^2$. As you can see, we are now able to quantitfy the dynamics of the system in three regimes: the exact phase ($\gamma < \gamma_{\mathcal{PT}}$), the spontaneous $\mathcal{PT}$-symmetry breaking point ($\gamma = \gamma_{\mathcal{PT}}$) and the broken phase ($\gamma > \gamma_{\mathcal{PT}}$).

2.2 Applications of $\mathcal{PT}$-Symmetry

Although we have discussed $\mathcal{PT}$-symmetry in the general framework of quantum mechanics, a promising application of $\mathcal{PT}$-symmetric systems appears in the framework of optics, where a medium with alternating regions of gain and loss can be synthesized, provided that the (complex) refractive index profile satisfies the condition $n^*(x) = n(x)$ [11, 22]. Experimental realizations of such systems have been reported in Refs. [13, 25] where

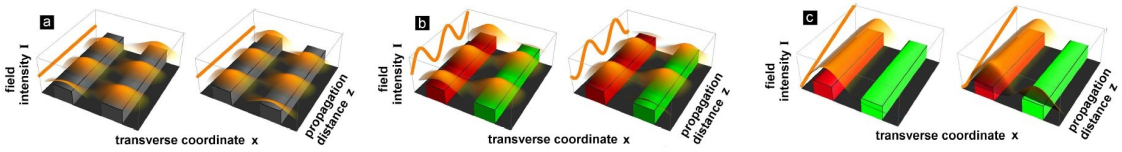

Figure 2.3: Numerical stimulation of of light beam propagation the active "$\mathcal{PT}$-symmetric system", where the spontaneous $\mathcal{PT}$-symmetry breaking is $\gamma_{\mathcal{PT}} = 1$. In figures a-c, the left/right panels correspond to an initial excitation at the left/right channel. The left (red) channel corresponds to the gain channel while the right (green) channel corresponds to the loss channel. (a) A total passive system corresponding to $\gamma = 0$. This propagation is reciprocal and the total intensity, I, remained constant throughout the propagation. (b) $\gamma < \gamma_{\mathcal{PT}}$ corresponding to the exact $\mathcal{PT}$-phase. In this case, we observed a non-reciprocality. (c) $\gamma > \gamma_{\mathcal{PT}}$ corresponding to the broken $\mathcal{PT}$-phase. The total intensity, I, is plotted with the logarithmic scale. Figure taken from [12].

a realization of the simple $\mathcal{PT}$ dimer, described by Eq. (2.1), was created and the beam dynamics was investigated. This kind of synthetic $\mathcal{PT}$ material was shown to exhibit all of the unique characteristics such as power oscillations, loss induced optical transparency, double refraction, and nonreciprocal dynamics, etc. that has been discussed in the previous section. Such intriguing properties of $\mathcal{PT}$-symmetric systems allow for a precise tailoring of light flow, and hence, the creation of on-chip integrated optical isolators [14], and of cloaking devices [26].

In this section, we will present an experimental realization of the two level system in the optics framework and highlight its main characteristics. Next, we will discuss a theoretical study that interplays the nonreciprocal dynamics arising from $\mathcal{PT}$ symmetry [13] with self-trapping phenomena associated with Kerr nonlinearities [27, 28]. We will show how this system serves as a mechanism for unidirectional optical transport because it can mold the flow of light in a surprising way.

2.2.1 Observations of $\mathcal{PT}$-dynamics in Photorefractive structures

Exotic properties such as intensity/power oscillations and non-reciprocal light propagation has been recently observed in $\mathcal{PT}$-symmetric system by C. E. Rüter et.al. [13].

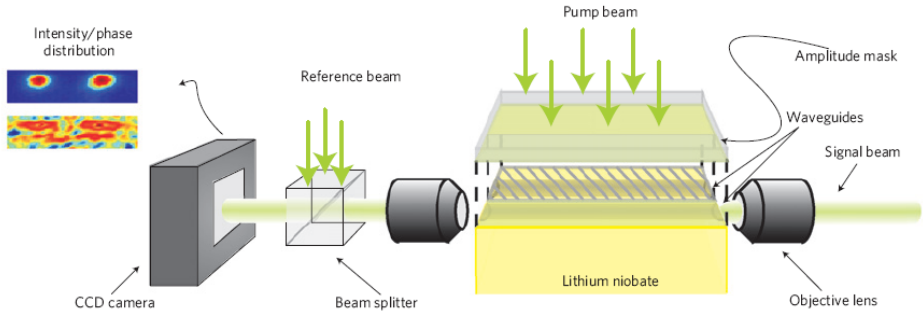

Figure 2.4: Experimental set-up. An Ar^+ laser beam is coupled into the arms of the structure fabricated on a photorefractive $LiNbO_3$ substrate. Waveguide 1 experience gain and the amplitude mask blocks the pump beam from entering into waveguide 2 which experience loss. The CCD camera at the end monitors the intensity and phases at the output. Figure taken from [13] and referenced herein.

The system studied consisted of two coupled $\mathcal{PT}$-symmetric waveguides fabricated from iron-doped $LiNbO_3$ as shown in Fig. 2.4. The Hamiltonian of this system corresponds to Eq. (2.1) where now, v_0 corresponds to the real part of the refractive index and κ is the evanescent coupling between the two waveguides. Each of the waveguides supports one propagating mode. One of these waveguides is being optically pumped to provide gain, γ_G, for the guided light, while the neighboring waveguide experiences an equal amount of loss, γ_L.

The beam dynamics results for this experiment is identical to the theoretical predictions discussed in section 2.1.2. These experimentally observed propagations are shown in Fig. 2.5.

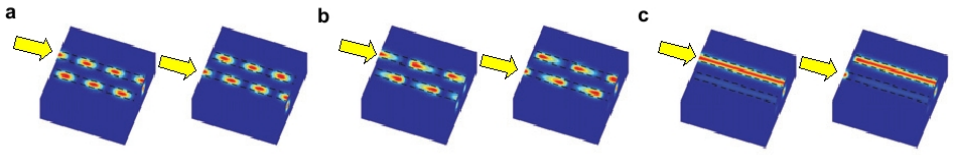

Figure 2.5: Experimental results of light beam propagation the active "$\mathcal{PT}$-symmetric system". In the above figures, the left/right panels correspond to an initial excitation at the left/right channel. The left channel corresponds to the gain channel while the right channel corresponds to the loss channel. (a.) A conventional system corresponding to $\gamma = 0$. This propagation is reciprocal. (b.) $\gamma < \gamma_{\mathcal{PT}}$ corresponding to the exact $\mathcal{PT}$-phase. In this case, we observed a non-reciprocality. (c.) $\gamma > \gamma_{\mathcal{PT}}$ corresponding to the broken $\mathcal{PT}$-phase. Figure taken from [13].

2.2.2 Unidirectional nonlinear $\mathcal{PT}$-symmetric optical structures

A particular interest in transport phenomena is to realize novel classes of integrated photonic devices that permit one-directional flow of information, e.g., optical isolators. Although the linear dimer (discussed in the previous section) exhibits non-reciprocal beam dynamics, the beam does not propagate in an unidirectional manner. Currently, unidirectional elements rely mainly on the Faraday effect, where external magnetic fields are used to break the space-time symmetry [14, 29]. In general, this requires materials with a big Verdet constant (*i.e.* an optical "constant "that describes the strength of the Faraday effect for a particular material). However, this value of the Verdet constant is typically incompatible with light-emitting wafers. Therefore, Ref. [14] states, "the the creation of optical diodes and isolators have been suggested. Some proposed models include the creation of optical diodes based on asymmetric nonlinear absorption [30], second harmonic generation in asymmetric waveguides [31, 32], nonlinear photonic crystals [33], and photonic quasicrystals and molecules [34, 35]".

In order to device a scheme that can fully suppresses the flow of light in one waveguide

while enhancing light propagation in the other, the authors of Ref. [14] introduced nonlinearity to the dimer discussed in the previous section. With nonlinearity, the beam propagates according to

$$\begin{aligned} i\frac{da(z)}{dz} + i\gamma a(z) + b(z) + \chi|a(z)|^2 a(z) = 0 \\ i\frac{db(z)}{dz} - i\gamma b(z) + a(z) + \chi|b(z)|^2 b(z) = 0 \end{aligned} \tag{2.11}$$

where χ is the strength of the Kerr nonlinearity and the coupling $\kappa = 1$.

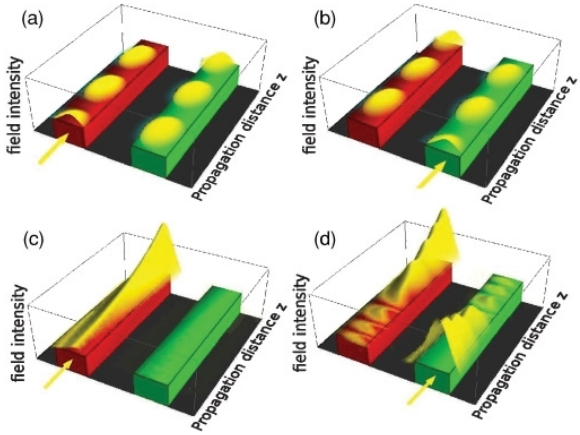

Figure 2.6: Beam propagation in two coupled nonlinear waveguides with nonlinearity strength χ and a complex $\mathcal{PT}$-symmetric refractive index profile. Waveguides are color coded, indicating balanced gain (red, left) and loss (green, right) regions ($\gamma = 0.1$). Left columns correspond to an initial excitation at the gain waveguide port, while right columns correspond to an initial excitation at the lossy waveguide. (a),(b) The nonlinearity $\chi = 1.9$ is below the critical value $\chi_d \approx 3.37$ while for (c) and (d) the nonlinearity strength $\chi = 8$ is above. Figure taken from [14] and referenced herein.

Examples of the resulting dynamics of this system is shown in Fig. 2.6, in which Fig. 2.6(a) and (b) corresponds to $\gamma = 0.1$ with nonlinearity strength $\chi = 1.9$ and (c) and (d) correspond to $\chi = 8$ with the same γ. Once again, it is clear from the figure that the introduction of gain/loss makes the dynamics nonreciprocal. However, by manipulating the strength of the nonlinearity, unidirectional propagation of the beam can

be obtained (as shown in Fig. 2.6c and d). This mean that the outgoing beam always leaves the sample from the gain waveguide irrespective of the waveguide from which the initial beam enters. Moreover, the beam intensity at the lossy waveguide approaches zero after a certain propagation distance along the waveguide. This novel unidirectional propagation of the $\mathcal{PT}$-symmetric nonlinear dimer is the key component in achieving optical diodes.

2.3 Summary

We have introduced the basic concepts of $\mathcal{PT}$-symmetry and presented some experimental (and technological) realizations of a new class of systems that although not $\mathcal{P}$ or $\mathcal{T}$ symmetric, they respect the combined $\mathcal{PT}$- symmetry. This chapter concluded with a theoretical work that combined $\mathcal{PT}$-symmetry with nonlinearity in order to make possible the realization of novel classes of integrated photonic diodes that allow an unidirectional beam transport.

Inspired by the novel unidirectional behavior that $\mathcal{PT}$ symmetry introduced in the field of optics, we wish to apply the same concept to thermal systems; where one of the technological challenges is to control heat transport.

Chapter 3

Basic Models and Theory of Heat Transport

Transport phenomena are central to many problems in physics, chemistry, and biology [36–39]. From the previous chapter, it is clear that transport properties are also of great technological interest because of their applications in a variety of transport-based devices such as optical isolators, rectifiers, pumps, particle separators, molecular switches, and electronic diodes and transistors. These applications can also be discussed in the framework of thermal transport as well.

In the thermal framework, energy transport in a solid is usually defined by the thermal conductivity, κ, defined via the Fourier's law

$$\mathbf{J}_Q = -\kappa \bigtriangledown T, \tag{3.1}$$

where the heat flux $\mathbf{J}_Q$ is the amount of heat transported through the unit surface per unit time and $T(\mathbf{x}, t)$ is the local temperature. The definition of these quantities, $\mathbf{J}_Q(\mathbf{x}, t)$ and $T(\mathbf{x}, t)$ relies on the local equilibrium hypothesis, *i.e.* the possibility to define a local temperature for a macroscopically small but microscopically large volume at each position $\mathbf{x}$ and time, t. Thus, beyond calculating the transport coefficient, a more

fundamental goal is to find the conditions in which local equilibrium can be realized and to ensure that a unique non-equilibrium stationary state can be attained on a physically accessible time scale. As Ref. [1] claims, "In this respect, simple mathematical models are an invaluable theoretical playground to provide a more firm foundation to heat conductivity and to understand more deeply the hypotheses underlying Eq. (3.1)."

This chapter aims to equip one with the basic tools necessary for understanding heat transport in thermal systems. In section 3.1.1, we will introduce the basic models used to study heat transport. Next, we will provide some basic definitions needed to describe heat transport, such as temperature, in section 3.1.2 and flux in section 3.1.3. Furthermore, we will discuss two heat-bath schemes that have been implemented in various studies. Namely, we will discuss a deterministic bath in section 3.2 and a stochastic bath in section 3.3. Finally, we will conclude in section 3.4.

3.1 Definitions

First, we will present some basic models and definitions of various observables that allow us to describe and study heat transport. This section follows closely the discussion provided in Ref. [1].

3.1.1 Models

For the simplicity of discussion, the models that we consider are one-dimensional. The generalization to two dimensions is straightforward and can be found in Ref. [1].

A schematic setup of the systems that will be discussed is illustrated in Fig. 4.1, where a chain of N coupled atoms is shown with the first and the last atoms interacting with a thermal bath. Let m_l and x_l be the mass and the position of the l^{th} particle, respectively. For simplicity, only nearest- neighbor interactions will be considered. The first model

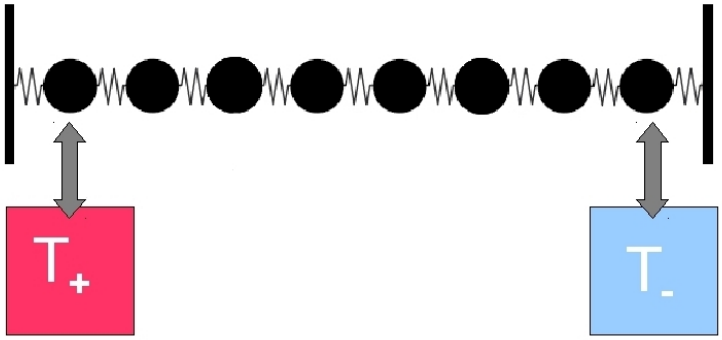

Figure 3.1: A schematic drawing of a chain of $N = 8$ coupled oscillators coupled with two thermal reservoirs at different temperatures.

that we will discuss has a Hamiltonian:

$$H = \sum_{l=1}^{N} \left[\frac{p_l^2}{2m_1} + V(x_{l+1} - x_l) \right]. \tag{3.2}$$

where $p_l = m_l \dot{x}_l$ is the momentum. This Hamiltonian can have boundary conditions that are either periodic, fixed, or free. Depending on the boundary conditions, one can then define x_0 and x_{N+1}. The total momentum of such system is conserved because only internal forces (*i.e.* forces that depend on relative positions) are present. In this case, a zero eigenvalue solution exists and the corresponding eigenfunction is known as the Goldstone mode. In the harmonic limit, the dispersion relation for the Hamiltonian in Eq. (3.2) admits an acoustic branch whose group velocity corresponds to the velocity of sound in the low wavenumber limit. Therefore, models of this type are often known as acoustic models.

There are two important examples for the potential that are worth mentioning. One of them is the well known Lennard-Jones potential:

$$V(z) = \epsilon[(\frac{a}{z})^{12} - 2(\frac{a}{z})^{6}] \tag{3.3}$$

where a is the equilibrium distance and ϵ is the well depth. The other example is the

Fermi-Pasta- Ulam (FPU) potential

$$V(z) = \frac{g_2}{2}(z-a)^2 + \frac{g_3}{3}(z-a)^3 + \frac{g_4}{4}(z-a)^4. \tag{3.4}$$

This potential results from expanding a generic (well behaved) potential, V, close to its equilibrium position $z = a$. There are special cases of this potential that are often used in literature. One of these cases is when $g_4 = 0$ and is known as the FPU-α model. In this model, small coupling constant g_3 and/or energies must be taken into account in order to avoid runaway instability of trajectories. The case where $g_3 = 0$ is known as the FPU-β model.

Although the Hamiltonian in Eq. (3.2) is simple, it does not model real crystals very well because it neglects the fact that real crystals are usually coupled to the environment. For example, artificial arrays of atoms are constructed by growing them on a substrate which exerts a pinning force on the atoms in such a way that stabilizes the lattice. Thus, a simple way to take this coupling into consideration is to include an external, on-site potential in the Hamiltonian

$$H = \sum_{l=1}^{N} \left[\frac{p_l^2}{2m_1} + U(x_l) + V(x_{l+1} - x_l) \right]. \tag{3.5}$$

Due to this external potential,$U(x_l)$, the total momentum is no longer conserved. Therefore, the branches of the dispersion relation have a gap at zero wavenumber. Models similar to (3.5) are known as optical models.

Before we proceed to discuss the basic definitions of temperature and flux, it is important to point out the units that we will employ. In the following sections, dimensionless variables will be used whenever possible. Therefore, the choice of the most natural units will depend on the specific model. For example, when considering the FPU model, it makes the most sense to set the equilibrium position a, mass m, and the angular frequency $\omega_0 = \sqrt{g_2/m}$ to one. This implies that the sound velocity, $a\omega_0$ is also one and thus, the energy is measured in units of $m\omega_0^2 a^2$.

3.1.2 Temperature

In order to interpret the molecular-dynamics simulations in the thermodynamical perspective, we first need to be able to define temperature in terms of dynamical variables. A rigorous definition of the temperature, which one can derive from the entropy, S, of system, is provided in Appendix C. The same definition can be obtained based on the virial theorem:

$$T = \langle \mathbf{u} \cdot \bigtriangledown H \rangle_{\mu} \tag{3.6}$$

where $\mathbf{u}$ is any vector that satisfies the condition $\bigtriangledown \cdot \mathbf{u} = 1$, where $\langle \cdot \rangle_{\mu}$ refers to the micro-canonical ensemble average. All of the units are chosen so that the Boltzmann constant is $k_B = 1$. Micro-canonical averages are used for the numerical investigation of isolated systems. Once heat baths are introduced into the system, canonical averages should be used instead. Fortunately, these two averages are the same in the thermodynamic limit. Furthermore, it is well known that the ensemble and time averages are equivalent in ergodic systems; thereby, allowing one to conveniently compute the averages by following a single trajectory over time.

According to Eq. (3.6), there are many different, but physically equivalent, definitions of the temperature. For example, the choice $\mathbf{u} = (0, \ldots, 0, p_1/N, \ldots, p_N/N)$ gives the definition of temperature adopted in the canonical ensemble:

$$T = \left\langle \frac{\sum_{i=1}^{N} p_i^2}{Nm} \right\rangle_{\mu}. \tag{3.7}$$

Another option is to choose $\mathbf{u} = (0, \ldots, 0, p_i, 0, \ldots, 0)$, which yields a local definition of temperature,

$$T = \left\langle \frac{p_i^2}{m} \right\rangle_{\mu} \tag{3.8}$$

3.1.3 Flux

This section aims to provide a meaningful definition of the heat flux. The heat flux $j(x,t)$ at time t in the spatial position x is the energy current, defined by the following

continuity equation

$$\frac{dh(x,t)}{dt} + \frac{\partial j(x,t)}{\partial x} = 0, \tag{3.9}$$

where $h(x,t)$ is the energy density. It must be pointed out that the energy flux defined above does not, in general, coincide with the heat flux because the former arises also from macroscopic motion [40]. Nonetheless, in solids and one-dimensional fluids, the two fluxes coincide and therefore both names are used interchangeably.

For an ensemble of interacting particles, we can write the microscopic energy density as the sum of the individual contributions located at the instantaneous position of each particle

$$h(x,t) = \sum_n h_n \delta(x - x_n), \tag{3.10}$$

where $\delta(x)$ is the Dirac distribution and

$$h_n = \frac{p_n^2}{2m_n} + U(x_n) + \frac{1}{2}\left[V(x_{n+1} - x_n) + V(x_n - x_{n-1})\right] \tag{3.11}$$

is the energy contribution of the n^{th} particle. The first term on the right hand side corresponds to the kinetic energy and the second term corresponds to the potential energy associated with the (possible) interaction with an external field. The last term is the potential energy that comes from the nearest neighbor interactions. Similarly, we can write the heat flux as the sum of individual contributions

$$j(x,t) = \sum_n j_n \delta(x - x_n). \tag{3.12}$$

But what is the definition of this local heat flux, j_n? We can find it by considering the energy flux in the limit of small oscillations around the equilibrium position. In this limit, the density fluctuation can be neglected and h_n is equal to the energy density times the lattice spacing, a. The time derivative of h_n can then be written as

$$\frac{dh_n}{dt} = m_n \dot{x}_n \ddot{x}_n + \dot{x}_n U'(x_n) - \frac{1}{2}\left[(\dot{x}_{n+1} - \dot{x}_n)F(x_{n+1} - x_n) + (\dot{x}_n - \dot{x}_{n-1})F(x_n - x_{n-1})\right], \tag{3.13}$$

where the prime denotes the derivative with respect to the argument and $F(x) = -V'(x)$ is the internal force. This expression can be further simplified by noting that the equation of motion for the optical model (Eq.(3.5)) can be written as

$$m_n \ddot{x}_n = -U'(x_n) - F(x_{n+1} - x_n) + F(x_n - x_{n-1}). \tag{3.14}$$

Substituting this expression into Eq. (3.13), one obtains

$$\frac{dh_n}{dt} = -\frac{1}{2}\left[(\dot{x}_{n+1} + \dot{x}_n)F(x_{n+1} - x_n) - (\dot{x}_n + \dot{x}_{n-1})F(x_n - x_{n-1})\right]. \tag{3.15}$$

Recalling continuity equation (Eq. (3.9)), we have

$$\frac{dh_n}{dt} + \frac{j_n - j_{n-1}}{a} = 0 \tag{3.16}$$

where

$$j_n = a\phi_n := \frac{1}{2}a(\dot{x}_{n+1} + \dot{x}_n)F(x_{n+1} - x_n) \tag{3.17}$$

is the definition of the local heat flux. The lattice spacing, $a \simeq x_{n+1} - x_n$ results from applying the chain rule to Eq. (3.15). Even if density fluctuations cannot be neglected, it has been shown in Ref. [1] that one still arrived at the above definition of the local heat flux.

3.2 Deterministic Bath

In order to discuss heat transport in any system, one needs to introduce a model of two heat baths coupled to a small system of interest. At equilibrium, this is usually accomplished by well known methods such as canonical molecular dynamics and Monte Carlo simulations [41]. However, out of equilibrium, one would need to consider non-equilibrium states of infinite systems. In the attempt to provide a self-consistent description of out-of-equilibrium processes, many types of deterministic baths have been introduced; one of the most successful schemes is the Nosé-Hoover thermostat [42]. The derivation of this thermostat starts from the extended system method and is discussed

in detail in Appendix D. As derived in Appendix D, the evolution of the particles in thermal contact with the bath α is governed by the set of equations

$$m\ddot{q}_n = F(q_n - q_{n-1}) - F(q_{n+1} - q_n) - \begin{cases} \xi_+ \dot{q}_n & \text{if } n \in S_+, \\ \xi_- \dot{q}_n & \text{if } n \in S_-, \end{cases} \tag{3.18}$$

where $\xi_\pm$ are two auxiliary variables modeling the microscopic action of the thermostat, and $S_\pm$ refer to the two sets of $N_\pm$ particles (at the beginning and the end of the chain, respectively) in contact with the baths.

The dynamics of $\xi_\pm$ is governed by the equation

$$\dot{\xi}_\pm = \frac{1}{\Theta_\pm^2} \left(\frac{1}{k_B T_\pm N_\pm} \sum_{n \in S_\pm} m\dot{q}_n^2 - 1 \right); \tag{3.19}$$

where $\Theta_\pm$ are the thermostat response times. The behavior of this thermostat can be understood in the following way. Whenever the temperature (*i.e.* the kinetic term) of the particles in $S_\pm$ is larger than $T_\pm$, $\xi_\pm$ increases and eventually becomes positive. Therefore, $\xi_\pm$ acts as a dissipation in Eq. (3.19). The opposite occurs when the temperature is below $T_\pm$ and this represents a stabilizing feedback around the given temperature.

Moreover, this scheme (as shown in Appendix D) reproduces the canonical equilibrium distribution. Deterministic thermostats such as this one possesses a Hamiltonian structure in an enlarged phase-space. An interesting property that is preserved by the projection onto the usual phase space is time-reversibility. It can be shown that the equations are invariant under time reversal

$$\dot{q}_n \to -\dot{q}_n \qquad n = 1, \ldots, N, \qquad \xi_\pm \to -\xi_\pm. \tag{3.20}$$

This property is the main reason that deterministic baths are successful; dissipation in such baths is not included a priori, but it follows self-consistently from the dynamical evolution. In particular, at equilibrium, $\langle \xi_\pm \rangle = 0$ indicates that the action of the bath does not break microscopic reversibility. Out of equilibrium, $\langle \xi_+ \rangle + \langle \xi_- \rangle > 0$ is due to entropy production.

3.3 Stochastic Bath

Another bath that is traditionally used is the stochastic bath. This bath introduced simultaneously random forces and dissipation according to the fluctuation-dissipation theorem.

We will arrive at the equations of motion for the chain of N particles by first considering the motion of a particle immersed in fluid and is subjected to Brownian motion (historically, the observation that small pollen grains are in a very animated and irregular state of motion when suspended in water). The equation of motion of a single particle system can described by the following Newton's equation:

$$m\ddot{x} = -\eta\dot{x} + \xi(t) \tag{3.21}$$

where $\dot{x}$ and $\ddot{x}$ corresponds to the particle's velocity and acceleration, respectively. η is proportional to the viscosity of the fluid. The force acting on the particle mass m at time t is a sum of a frictional force proportional to the particle's velocity, and a noise term, $\xi(t)$, which represents the effect of the collisions of the particle with surrounding molecules in the fluid. Since $\xi(t)$ corresponds to white noise, it has a mean of

$$\langle \xi(t) \rangle_\xi = 0 \tag{3.22}$$

and an autocorrelation of

$$\langle \xi(t+\tau)\xi(t) \rangle_\xi = \sigma^2 \delta(\tau). \tag{3.23}$$

where σ^2 is the variance of the Gaussian probability distribution and has a value of $\sigma^2 = 2\lambda k_B T$. One attempt to solve Eq. (3.21) is to write it in the following Langevin form

$$\begin{aligned} \dot{x} &= v \\ \dot{v} &= -\lambda v + f(t) \end{aligned} \tag{3.24}$$

where $\lambda = \eta/m$ and $f(t) = \xi(t)/m$. An explicit formal solution of this equation is given by

$$v(t) = v_0 e^{-\lambda t} + \int_0^t e^{-\lambda(t-s)} f(s) ds \tag{3.25}$$

To make some physical sense of this solution, it's important to examine the first and second moments of the velocity. The first moment of velocity is given by

$$\langle v(t) \rangle_\xi = v_0 e^{-\lambda t} + \int_0^t e^{-\lambda(t-s)} \langle f(s) \rangle_\xi ds \tag{3.26}$$

Since $\langle f(s) \rangle_\xi = 0$ according to Eq. (3.22), the first moment simplifies to

$$\langle v(t) \rangle_\xi = v_0 e^{-\lambda t} \tag{3.27}$$

In the long time limit, this quantity goes to zero. This matches our intuition that $\overline{\langle v(t) \rangle_\xi} = 0$, in which the overline corresponded to an average over the initial velocities.

In order to obtain the second moment, we introduced the correlation function

$$C_v(t_2 - t_1) = \langle (v(t_2) - \langle v(t_2) \rangle) \cdot (v(t_1) - \langle v(t_1) \rangle) \rangle_\xi \tag{3.28}$$

After some algebra shown in Appendix E, the correlation function becomes

$$C_v = \frac{\sigma^2}{2\lambda} \{ e^{-\lambda |t_1 - t_2|} - e^{-\lambda(t_1 + t_2)} \}. \tag{3.29}$$

Once we recall that $C_v = \langle v^2(t) \rangle - \langle v(t) \rangle^2$, we can write the second moment as

$$\langle v^2(t) \rangle = C_v(0) + \langle v(t) \rangle^2. \tag{3.30}$$

Substituting in the expression for the correlation function and the square of the moment gives

$$\langle v^2(t) \rangle = \frac{\sigma^2}{2\lambda} + e^{-2\lambda t} \left(v_0^2 - \frac{\sigma^2}{2\lambda} \right). \tag{3.31}$$

According to the equipartition theorem, every square term in the Hamiltonian contributes $\frac{1}{2} k_B T$ to the energy, *i.e.* $\frac{1}{2} m \langle v^2 \rangle = \frac{1}{2} k_B T$. Thus, we are expecting the second moment to scale as $k_B T$. In thermal equilibrium, where there is no t-dependence,

$\left(v_0^2 - \frac{\sigma^2}{2\lambda}\right) = 0$. Therefore, by noting that $\frac{\sigma^2}{2\lambda} = k_B T$, we obtain the following fluctuation-dissipation relation

$$\lambda = \frac{\sigma^2}{2k_B T}, \tag{3.32}$$

which relates the strength, σ^2, of the fluctuating force to the magnitude, λ, of the dissipation.

Similarly, one can elevate this one particle system to a many particle system. In the simple case of an equal-mass chain, the equation of motion is governed by the following set of Langevin equations:

$$m\ddot{q}_n = F(q_n - q_{n-1}) - F(q_{n+1} - q_n) + (\xi_+ - \lambda_+ \dot{q}_n)\delta_{n1} + (\xi_- - \lambda_- \dot{q}_n)\delta_{nN}, \tag{3.33}$$

where $\xi_\pm$'s are again the noise term with zero mean and variances $2\lambda_\pm k_B T_\pm$. The plus and minus sign corresponds to the different temperatures in the bath coupled to the first and last site of the chain, respectively.

A way to implement the stochastic bath is to picture each reservoir as a one-dimensional ideal gas of particles of mass $M_\pm$ interacting with the chain through elastic collisions. First, a random set of initial positions and velocities is chosen for the atoms in the chain. Next, the equations of motion are used to advance the time t, by an increment δt. Numerically, this is done by implicit integration procedures such as the Runge-Kutta. The increment δt is chosen to be small compared to the minimum vibration period of the lattice. With some probability $\Lambda \delta t$, each of the end atoms experience a collision with an atom in its respective reservoir and impulsively gain a momentum increment. This results in

$$\dot{q}_1 \to \dot{q}_1 + \frac{2M_+}{m + M_+}(v - \dot{q}_1) \tag{3.34}$$

for the left reservoir. Likewise, an analogous expression holds for the right reservoir. The collision probability Λ is a preassigned constant, independent of the velocities. The initial velocity, v, of the gas particle is a random variable chosen according to a

Maxwellian distribution

$$P_+(v) = \sqrt{\frac{M_+}{2\pi k_B T_+}} \exp\left(-\frac{M_+ v^2}{2k_B T_+}\right) \tag{3.35}$$

In the case where $M_\pm = m$, the process is simply an exchange of velocities between the particles. In the case that $M_\pm \ll m$, the interaction with the reservoirs yields the Langevin equation in Eq. (3.33) with $\lambda_\pm = 2M_\pm/\bar{t}$, where $\bar{t}$ is the average collision time.

This method is computationally simple because it does not deal with the stochastic differential equations. Moreover, the dissipation is not included a priori in the model but is self-consistently generated by the dynamics.

There are many other schemes for the heat baths that were not discussed in this thesis. One may refer to Ref. [1] for more informations on these schemes.

3.4 Summary

We have introduced the basic models used to study heat transport in thermal systems and provided the definitions of the necessary quantities such as local temperature and flux. Furthermore, we discussed the most commonly used heat baths – the deterministic baths and stochastic baths and showed how fluctuation and dissipation is incorporated in both. In the following chapter, we will use these tools to study heat transport in a novel system that we will propose.

Chapter 4

Transport in $\mathcal{PT}$-Symmetric Harmonic Chains

Up to now, all the theoretical studies of energy transport on the nano-scale level have been conducted on *passive* (conservative) systems [1], that is, systems without any active elements which would amplify or dissipate local energy from or to some external degrees of freedom. However, dissipation mechanisms are inevitable in practical applications and thus one of the key challenges encountered in thermal engineering is their presence, that typically degrades the efficiency of thermal devices. As a result, considerable research effort is invested in eliminating and mitigating these undesirable absorption mechanisms. Below, we adopt the opposite viewpoint: we suggest to manipulate absorption, and via a judicious design that involves the combination of amplification and absorption regions, we achieve new schemes of thermal conduction with intriguing properties similar to thermal rectification and heat switching. Our study is inspired by recent achievements in the field of optics, where it has been discovered [11] that a new class of synthetic materials (so-called $\mathcal{PT}$ meta-materials) created by delicately balanced amplification and absorption regions can exhibit novel properties [11–14]. At the heart of these innovative ideas is the observation that non-Hermitian Hamiltonians that respect the

combined parity ($\mathcal{P}$) and time ($\mathcal{T}$) reversal symmetry can have a real spectrum and thus generate a (pseudo)-unitary time evolution [15, 16, 43–46].

In this chapter, we present a theoretical study of heat transport through an *active harmonic chain* coupled at the left and right edges to a pair of Langevin heat reservoirs with temperatures T_L and T_R, respectively. The main result of this study has been recently submitted for publication [10]. First, the model and mathematical formalism will be introduced in section 4.1. Next, we will present a simple two oscillator system that is analytically solvable in section 4.1.3. Section 4.2 will investigate the the system that we proposed, while an analytical understanding will be discussed in the section 4.2.2. Finally, we conclude with a proposal for an electronic implementation in section 4.3 and a summary in section 4.4.

4.1 Model and Mathematical Formalism

The mathematical model that we consider is schematically illustrated in Fig. 4.1. It consists of a chain of $N = N_a + 2N_b$ particles of equal mass m coupled by harmonic springs of constant k. The first (last) N_b particles are coupled to a Langevin reservoir of temperatures T_L (T_R). We assume that the coupling constant κ with the reservoirs is the same for all particles. We also have two active oscillators, an amplifier - where the motion is linearly amplified - and an attenuator - where it is linearly damped - placed symmetrically with respect to the middle of the chain, at positions n_γ and $n_{-\gamma}$ respectively. Choosing units in which $m = k = 1$, the corresponding stochastic equations of motion are

$$\begin{aligned}
\frac{dq_n}{dt} &= p_n; \qquad n = 1, \dots N \\
\frac{dp_n}{dt} &= q_{n+1} - 2q_n + q_{n-1} + \sum_{\sigma=\pm} \sigma\gamma\delta_{n,n_{\sigma\gamma}} p_n + \sum_{\tau=L,R} (-\kappa p_n + \sqrt{2\kappa T_\tau})\theta_n^\tau \xi_n. \qquad (4.1)
\end{aligned}$$

with open boundaries ($q_0 \equiv q_{N+1} \equiv 0$), $\theta_n^L = \{1 \text{ if } n \leq N_b; 0 \text{ otherwise}\}$, $\theta_n^R = \{1 \text{ if } n > N_a + N_b; 0 \text{ otherwise}\}$, and $\xi_n(t)$ delta-correlated Gaussian stochastic variables with

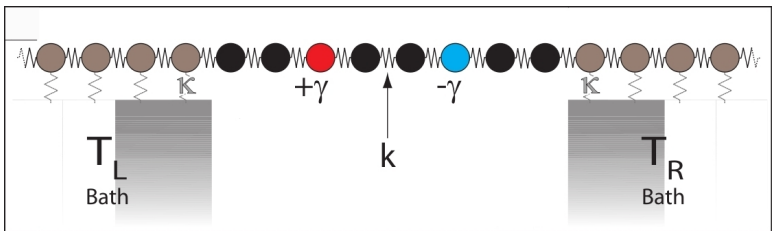

Figure 4.1: (a) Schematic illustration of an active harmonic chain model: $N_a = 8$ harmonic masses are, coupled to two other large sub-lattices which are in turn coupled to Langevin baths. Figure taken from Ref. [10] and referenced herein.

$\langle \xi_n(t)\xi_{n'}(t')\rangle = \delta_{n,n'}\delta(t-t')$ where the bracket represents a noise average.

4.1.1 Mathematical Formalism for $\kappa = 0$

For $\kappa = 0$, the system of N coupled oscillators is isolated from the reservoirs. In this case, the Hamiltonian associated with Eqs. (4.1) is $\mathcal{PT}$-symmetric [15, 43]. The normal modes and eigenfrequencies can be calculated by performing the substitution $q_n^\alpha = A_n \exp(\lambda_\alpha t)$. In accordance to the standard $\mathcal{PT}$-scenario [15, 18, 19, 43] discussed in Chapter 2, we find that the eigenfrequencies λ_α are imaginary for an amplification/attenuation parameter γ smaller than a critical value $\gamma_{\mathcal{PT}}$. In this regime the normal modes are also eigenmodes of the $\mathcal{PT}$ operator. For $\gamma > \gamma_{\mathcal{PT}}$ the eigen-frequencies of the system are complex while the normal modes are no longer eigenstates of the $\mathcal{PT}$ operator. The eigenvalues for these two regimes are plotted in Fig. 4.2, where blue corresponds to the real eigenfrequencies and red corresponds to the corresponding imaginary part. As discussed in Chapter 2, γ_{PT} is the first point where two real eigenfrequencies coalesce resulting in two complex ones.

However, once we introduce the coupling to the thermal reservoirs (*i.e.* $\kappa \neq 0$), a different mathematical formalism is required in order to understand the behavior of the added stochastic term.

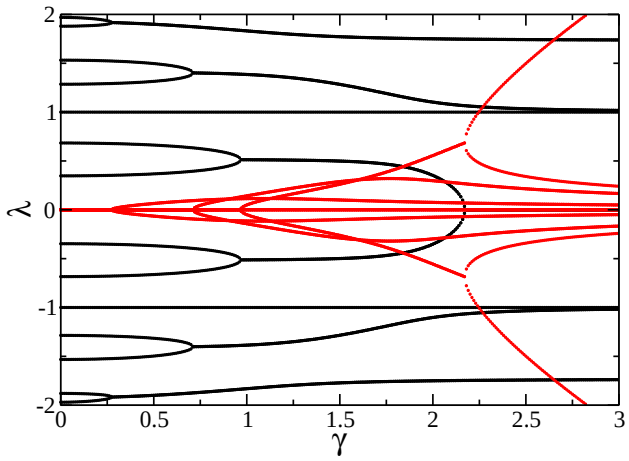

Figure 4.2: The real and imaginary part of the eigenfrequencies Vs. the amplification/attenuation parameter,γ. The black lines denote the real eigenfrequencies (*i.e.* imaginary λ_α) and the red lines denote the corresponding imaginary part (*i.e.* real part of λ_α). The blue line marks where $\gamma_{\mathcal{PT}}$ is.

4.1.2 Mathematical Formalism for $\kappa \neq 0$

For $\kappa \neq 0$, we use Ito calculus of stochastic differential equations and derive (in Appendix F) the equation of motion for the covariances $\mathbf{C}(\mathbf{t}) = \langle \tilde{\mathbf{x}}(\mathbf{t}) \otimes \tilde{\mathbf{x}}(\mathbf{t}) \rangle$, where the vector $\vec{x}$ is defined as $\vec{x} = (q_1, \ldots, q_N, p_1, \ldots, p_N)^T$. We find

$$d\mathbf{C}/dt = \mathbf{Z}\mathbf{C} + \mathbf{C}\mathbf{Z}^T + \mathbf{Y} \tag{4.2}$$

where $\mathbf{Z}$, and $\mathbf{Y}$ are $2N \times 2N$ matrices

$$\mathbf{Z} = \begin{pmatrix} \mathbf{0} & \mathbf{1} \\ \mathbf{D} & \mathbf{0} \end{pmatrix} + \sum_{\sigma=\pm} \sigma\gamma \mathbf{P}_{N+n_\sigma} - \sum_{\tau=L,R} \mathbf{Y}^\tau \tag{4.3}$$

$$\mathbf{Y} = \sum_\tau T_\tau \mathbf{Y}^\tau, \quad \text{with } \mathbf{Y}^\tau = \kappa \sum_{n=1}^{N} \theta_n^\tau \mathbf{P}_{N+n}. \tag{4.4}$$

Above, $\mathbf{P}_k = \vec{e}_k \otimes \vec{e}_k$ are diagonal rank-1 projectors, $\mathbf{e}_k$ is a basis vector with elements $(\vec{e}_k)_n = \delta_{n,k}$ and $\mathbf{D}$ is an $N \times N$ matrix with elements $D_{n,m} = -2\delta_{n,m} + \delta_{n,m+1} + \delta_{n,m-1}$

which encodes all the physical information about the interactions within the harmonic lattice.

For this system, we are interested in the non-equilibrium steady state (NESS), whose covariance matrix $\mathbf{C}_\infty$ satisfies the following Lyapunov equation

$$\mathbf{Z}\mathbf{C}_\infty + \mathbf{C}_\infty\mathbf{Z}^T = -\mathbf{Y} \tag{4.5}$$

The existence and the stability of the NESS are determined by the (complex) spectrum $\{\lambda_\alpha, \alpha = 1, \ldots, 2N\}$ of the real non-symmetric matrix $\mathbf{Z}$, [1] defining a bi-orthonormal set of right $\vec{v}_\alpha$ and left $\vec{v}'_\alpha$ eigenvectors,

$$\mathbf{Z}\vec{v}_\alpha = \lambda_\alpha\vec{v}_\alpha, \quad \mathbf{Z}^T\vec{v}'_\alpha = \lambda_\alpha\vec{v}'_\alpha, \quad \vec{v}_\alpha \cdot \vec{v}'_\beta = \delta_{\alpha,\beta}. \tag{4.6}$$

In other words, NESS exists if all eigenvalues λ_α have *negative real part*, $\Re\lambda_\alpha < 0$. Otherwise, if for some, α, $\Re\lambda_\alpha > 0$, the time-dependent covariances (4.2) - for a generic initial condition - increase as $\exp(2t\Re\lambda_\alpha)$ signaling an uncontrolled amplification of the system. The transition to unstable behavior is determined by the parameter γ. We define γ_i, as the point for which the first eigenvalue reaches the line $\Re\lambda_1(\gamma = \gamma_i) = 0$.

Our formalism can be utilized to derive the properties of NESS. For example, the temperature $T_n = \langle p_n^2 \rangle$, at each site corresponds to $C_{n+N,n+N}$ and the energy current at site n is a linear combination of the covariance matrix elements, *i.e.*

$$J_n = \frac{\langle p_n(q_{n+1} - q_{n-1})\rangle}{2} = \frac{(C_{n+1,n+N} - C_{n-1,n+N})}{2} \tag{4.7}$$

Furthermore, since the matrix $\mathbf{Y}$ on the RHS of Eq. (4.5) is *linear* in the two bath temperatures T_τ, its solution - the full covariance matrix - and hence all the currents, are also linear in T_τ, namely

$$\mathbf{C}^\infty = T_L\mathbf{C}^L + T_R\mathbf{C}^R \tag{4.8}$$

[1] We order the eigenvalues w.r.t. non-increasing real part $\Re\lambda_\alpha \geq \Re\lambda_\beta$ for $\alpha < \beta$. Moreover, since $\mathbf{Z}$ is real, the corresponding eigenvalues come in complex conjugate pairs $\lambda_{2k} = \lambda^*_{2k-1}$.

where $\mathbf{C}^\tau$ solves the *temperature independent* Lyapunov equations $\mathbf{Z}\mathbf{C}^\tau + \mathbf{C}^\tau\mathbf{Z}^T = -\mathbf{Y}^\tau$. If J_L and J_R designate the energy/heat currents in NESS to the left and right baths respectively, *i.e.* $J_L = J_n^\infty$, for $N_b < n < n_{\sigma\gamma}$, and $J_R = J_n^\infty$ for $n_{\sigma\gamma} < n \leq N_a + N_b$ (since J_n^∞ is site independent for passive sites uncoupled from the baths due to energy conservation) then we may write

$$J_\tau = K_L^\tau T_L + K_R^\tau T_R \tag{4.9}$$

where $K_{\tau'}^\tau \equiv \partial J_\tau / \partial T_{\tau'}$ are temperature independent coefficients obtained explicitly combining (4.8) and (4.9).

Now that we developed the tools necessary to observe the temperature profile and flux of the system, we will illustrate the implementation of this formalism via the simplest system, which corresponds to $N = 2$.

4.1.3 Dimer example

The above mentioned theoretical analysis is best illustrated by a simple dimer (*i.e.* $N = 2$). The model is shown schematically in Fig. 4.3.

The equation of motion for this system corresponds to

$$\dot{p}_\alpha = q_{\bar{\alpha}} - 2q_\alpha + [(-1)^\alpha\gamma - \kappa]p_\alpha + \sqrt{2\kappa T_{bath}^\alpha}\xi_\alpha \tag{4.10}$$

where α denotes sites 1 or 2 and $\bar{\alpha}$ denotes the complementary site. This equation of motion can be rewritten by defining the vector $\vec{x}$ as follow

$$\vec{x} = \begin{pmatrix} q_1 \\ q_2 \\ p_1 \\ p_2 \end{pmatrix}. \tag{4.11}$$

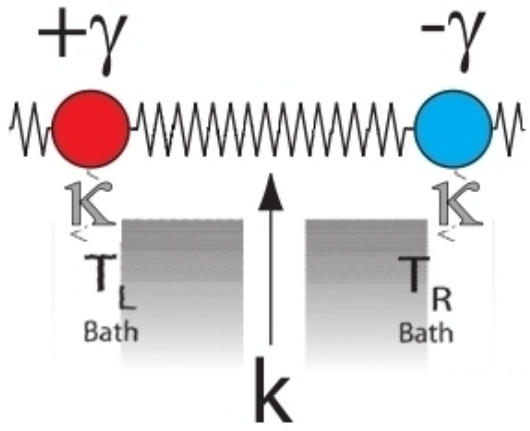

Figure 4.3: A schematic illustration of an active harmonic dimer model: $N = 2$ harmonic masses are coupled to each other and to Langevin baths. $+\gamma$ corresponds to the the amplifier and $-\gamma$ denotes the attenuator.

The equation of motion can then be express in the following matrix form

$$\frac{d\vec{x}}{dt} = \underbrace{\begin{pmatrix} 0 & 0 & 1 & 0 \\ 0 & 0 & 0 & 1 \\ -\beta - a & 1 & \gamma - \kappa & 0 \\ 1 & -\beta - a & 0 & -\gamma - \kappa \end{pmatrix}}_{\mathbf{Z}} \vec{x} + \underbrace{\begin{pmatrix} 0 & 0 & 0 & 0 \\ 0 & 0 & 0 & 0 \\ 0 & 0 & \sqrt{2\kappa T^1_{bath}} & 0 \\ 0 & 0 & 0 & \sqrt{2\kappa T^2_{bath}} \end{pmatrix}}_{\mathbf{D}} \begin{pmatrix} 0 \\ 0 \\ \xi_1 \\ \xi_2 \end{pmatrix}. \tag{4.12}$$

The stationary properties of this system (*i.e.* the eigenvalues and eigenvectors) can be found via a direct diagonalization of the **Z** matrix, the latter being nothing else than the Liouvillian matrix.

Spectra Analysis

For $\kappa = 0$, the standard scenario of $\mathcal{PT}$-symmetry breaking is observed and illustrated in Fig. 4.4.

Once κ is introduced, a single pair of eigenvalues $\lambda_{1,2}$ starts from negatives and becomes

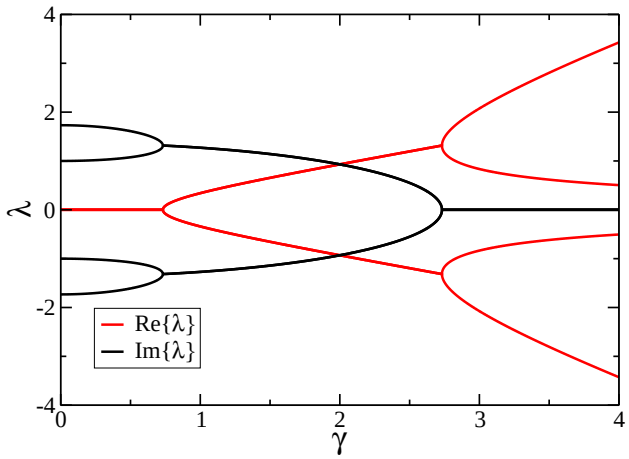

Figure 4.4: The real and imaginary part of the eigenfrequencies Vs. the amplification/attenuation parameter,γ for $N = 2$ and $\kappa = 0$. The black lines denote the real eigenfrequencies (*i.e.* $\Im\lambda$) and the red line denote the corresponding imaginary part (*i.e.* $\Re\lambda$).

positive at $\gamma = \gamma_i$, where above γ_i, we have instability in the system (as shown in Fig. 4.5). It is important to note that introducing the coupling to the baths still allow a region of stability with the width of this region controlled by the coupling strength κ.

The coupling of the system to the bath, κ, acts as a type of perturbation. It not only lifts the degeneracies, but it also shifts the real part of the energies down to the negative semi-plane, by a factor proportional to κ. Compared to the closed system, the open system has a smaller region of stability. However, this region increases with increasing κ (see Fig. 4.6). Since we treat κ as some sort of perturbation, only small values of κ's are considered. Physically, it also makes sense since large κ values correspond to a large collision rate (where the dynamics of the system become dominated by the baths.)

Not only is the region of stability affected by κ, but the imbalance between the am-

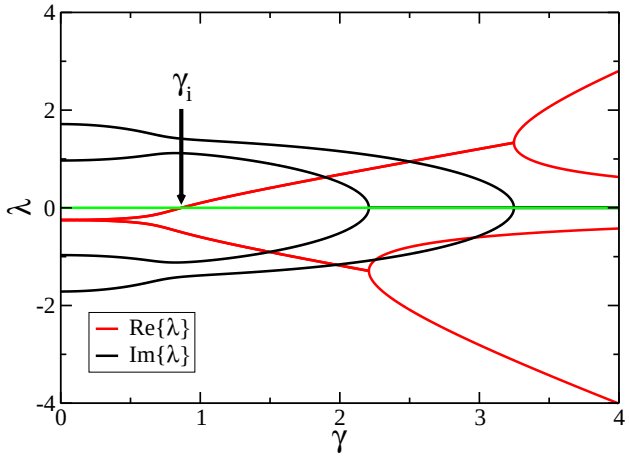

Figure 4.5: The real and imaginary part of the eigenfrequencies Vs. the amplification/attenuation parameter,γ for $N = 2$, $\kappa = .5$. The black lines denote the real eigenfrequencies (*i.e.* $\Im\lambda$) and the red lines denote the corresponding imaginary part (*i.e.* $\Re\lambda$).

plification and attenuation also plays a role. Instead of having the amplification and attenuation be of equal magnitude, we allow the amplification to stay the same (*i.e.* $+\gamma$) while the attenuation becomes $-\gamma(1-\Delta)$, where Δ serves as an off-set from $\mathcal{PT}$-symmetry. As the system deviates from $\mathcal{PT}$-symmetry, the region of stability decreases (see Fig. 4.6). Since we are interested in a system that exhibits a large region of stability, we will only consider systems in which the amplification and attenuation are places in a $\mathcal{PT}$-symmetric manner.

Analysis of the dynamical properties

As mentioned in the section 4.1.2, we can extract the steady state properties (such as the temperature profile and flux) of our system from the covariance matrix $\mathbf{C}$. The steady state solution of Eq. (4.12) yields a covariance matrix $\mathbf{C}$, whose temperatures on

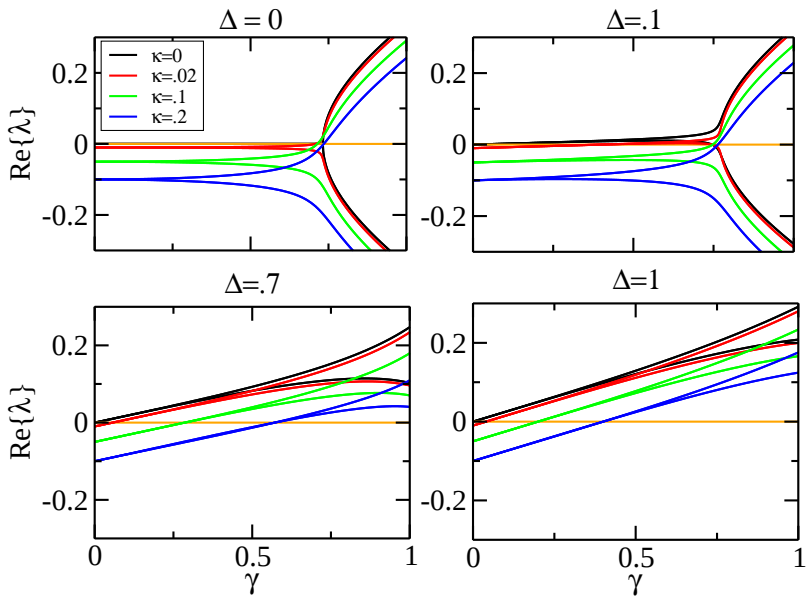

Figure 4.6: λ Vs. γ for $N = 2$. Each sub-figure corresponds to a different value of the off-set Δ. $\Delta = 0$ corresponds to the $\mathcal{PT}$-symmetric case and $\Delta = 1$ corresponds to the case where there is amplification, but no attenuation.

sites 1 and 2 correspond to C_{33} and C_{44} matrix elements, respectively:

$$T_1 = C_{33} = \frac{T_R + T_L(1 + 4\gamma\kappa + 4\kappa^2)}{2 - 4\gamma^2 + 4\kappa^2}; \qquad T_2 = C_{44} = \frac{T_L + T_R(1 - 4\gamma\kappa + 4\kappa^2)}{2 - 4\gamma^2 + 4\kappa^2} \tag{4.13}$$

Here, T_L and T_R corresponds to the left and right temperature of the bath, respectively. Note that the added amplifier and attenuator allow T_1 and T_2 to be *non-reciprocal*, similar to the behavior in the dynamics of the optical dimer.

For the dimer, we can find the analytical expression for the γ_i by noting that it is the point above which we no longer have a steady temperature profile. From Eq. (4.13), this occurs when the denominator approaches zero (*i.e.* $2 - 4\gamma^2 + 4\kappa^2 = 0$). Therefore, we obtain the following expression for γ_i

$$\gamma_i = \sqrt{\frac{1}{2} + \kappa^2}. \tag{4.14}$$

The flux for this system cannot be defined using the standard definition of flux given in Eq. (4.7). However, we can conjecture the flux going into the left and right bath to be $J_L = C_{33} - T_L$ and $J_R = C_{44} - T_R$, respectively.

To a zeroth order approximation, we obtain the following functional form for the left and right flux:

$$\begin{aligned} J_L &= \frac{1}{\delta\gamma}(c_1 T_L + c_2 T_R) + (c_3 T_R - c_4 T_L) + O[\delta\gamma]^1 \\ J_R &= \frac{1}{\delta\gamma}(q_1 T_L + q_2 T_R) + (q_3 T_L - q_4 T_R) + O[\delta\gamma]^1 \end{aligned} \tag{4.15}$$

where, $\delta\gamma = \gamma_i - \gamma$ and c's and q's are some constants. The last term in both equations is the first order approximation. This functional form tells us two different behaviors of the fluxes. For $\gamma << \gamma_i$, The second term in the fluxes dominate. In this case, as we increase T_L (T_R), while keeping the other bath T_R (T_L) at constant temperature, we expect to see a *decrease* in the flux flowing into the left (right) bath. This case matches our intuition that heat flows from high to low. However, once γ approaches γ_i, the first term determines the flux behavior. In this case, these equation tell us that we'll observe an opposite behavior from the previous case. Namely, as we increase T_L (T_R), while keeping the other bath T_R (T_L) at constant temperature, we expect to see an *increase* in flux flowing into the left (right) bath (*i.e.* the hotter the bath temperature, the more flux flows to it!). This counterintuitive prediction from the simple dimer motivated us to study a slightly more extended system where we can numerically measure these fluxes.

4.2 Beyond the Dimer

Although the simple dimer model offer us a preliminary insight on the effect of including active elements into harmonic chains coupled to Langevin baths, it fail to provide us a ground to measure and confirm our theoretical conjecture of the flux behaviors. Therefore, we must elevate our model to the one depicted in Fig. 4.1. In this model, the

two passive sites to the left, right, and in between the amplifier and attenuator allow us to measure the fluxes defined in Eq. (4.7).

4.2.1 Spectra Analysis

Similar to the case of the dimer, we found that a $\mathcal{PT}$-symmetric configuration results in an increase of the stable γ-domain. In the main panel of Fig. 4.7a we show, the parametric evolution of λ_α as a function of γ for the $\mathcal{PT}$ configuration of Fig. 4.1. We note that most of the eigenvalues are located inside a band, and remain unchanged as γ increases. Only a single pair of eigenvalues $\lambda_{1,2}$ is approaching and crossing the imaginary line at $\gamma = \gamma_i$. Such behavior is typical of $\mathcal{PT}$-symmetric systems. In the upper inset of Fig. 4.7a, we show the behavior of γ_i versus the coupling parameter κ and various bath sizes N_b. In all cases, $\gamma_i \leq \gamma_{\mathcal{PT}}$, while for large κ's the critical γ_i reaches an asymptotic value. Finally in Fig. 4.7b we show for comparison, the spectrum of a non-$\mathcal{PT}$-symmetric structure, where $\gamma_L = \gamma$ and $\gamma_R = 0$. Among the various non-$\mathcal{PT}$ configurations that we have tested, it provides the most noticeably smaller value of γ_i than the one found in Fig. 4.7a.

4.2.2 Analysis of dynamical properties

For $\gamma = 0$, clearly $J_L = -J_R$ and $K_L^L > 0$, $K_R^R < 0$. However, for an active system a critical γ_τ^*, $0 < \gamma_\tau^* < \gamma_i$, may exist for which one of the currents J_τ does not depend on the corresponding temperature T_τ and thus the *differential thermal conductance* vanishes $K_\tau^\tau|_{\gamma=\gamma_\tau^*} = 0$. This is nicely illustrated by our numerical data in Fig. 4.8. Moreover, as γ increases above γ_τ^*, the differential thermal conductance K_τ^τ changes sign. Specifically, we found that $K_L^L(\gamma < \gamma_L^*) > 0$ ($K_R^R(\gamma < \gamma_R^*) < 0$ while $K_L^L(\gamma > \gamma_L^*) < 0$ ($K_R^R(\gamma > \gamma_R^*) > 0$. Thus, in the interval $\gamma_L^* < \gamma < \gamma_R^*$ both differential thermal conductances K_L^L, K_R^R are negative. While for $\gamma < \gamma_\tau^*$ the heat flow is consistent with the standard expectations, the opposite limit of $\gamma > \gamma_\tau^*$ is counter-intuitive. Specifically,

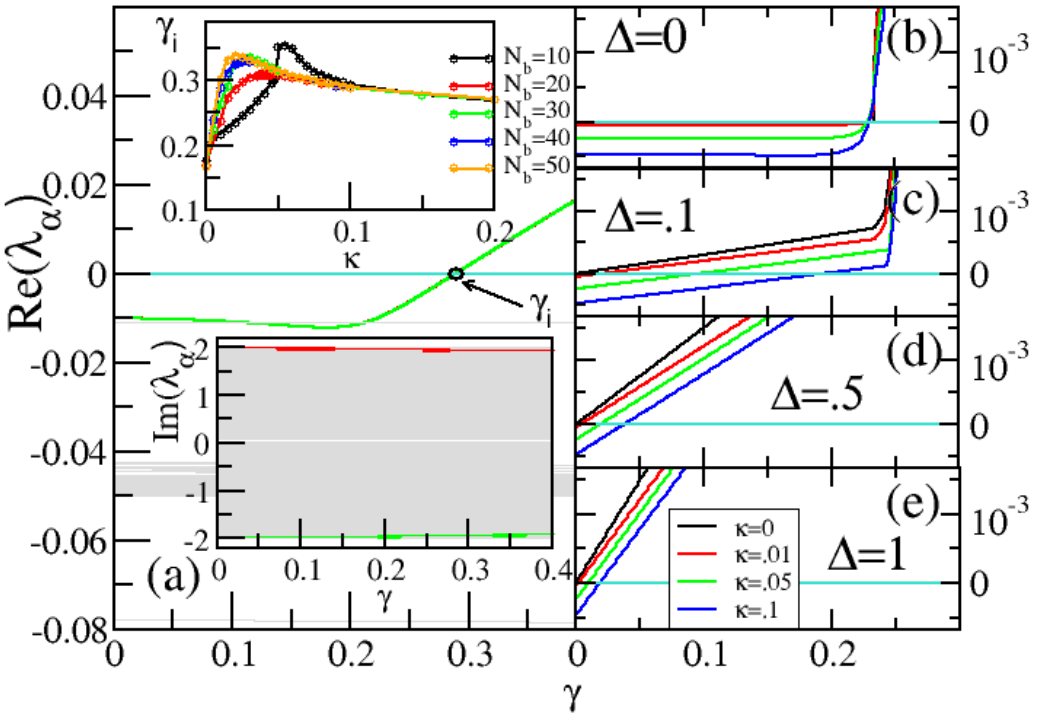

Figure 4.7: (a) The real and the imaginary (lower inset) part of the spectrum λ of the $\mathcal{PT}$-symmetric harmonic chain of Fig. 4.1, vs. the amplification/attenuation parameter γ. The green (red) curve corresponds to the leading eigenvalue, $\Re\lambda_1$ ($\Im\lambda_1$). The upper inset shows the instability point γ_i vs. the bath coupling constant κ for various N_b-values. (b)-(e) The same as in (a), but now for only the pair of eigenfrequencies that contributed toward the instability of the system are shown for different values of κ for different values of the imbalance, Δ.

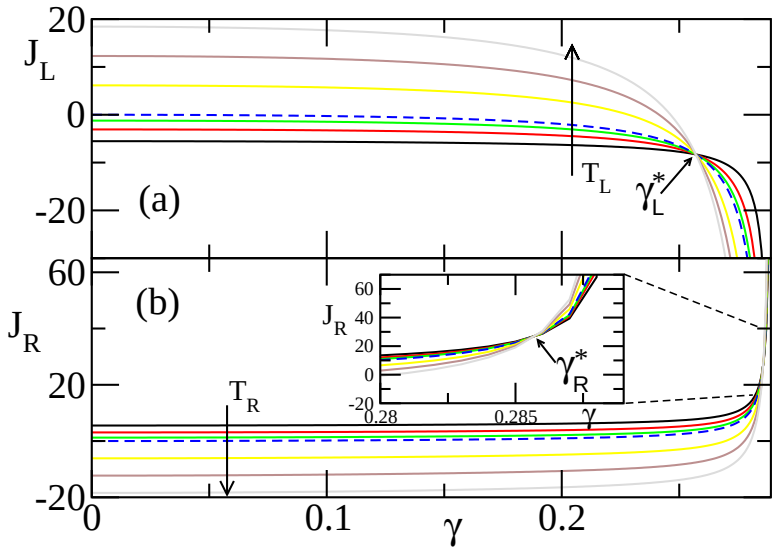

Figure 4.8: (a) Heat flux J_L as a function of the parameter γ for various T_L temperatures and fixed $T_R = 10$; (b) Heat flux J_R for various T_R temperatures and fixed $T_L = 10$. In the inset we show a magnification of the area around γ_R^*. The dashed blue lines correspond to heat fluxes for the case where $T_L = T_R$. A non-reciprocal behavior is obvious.

we find that $J_L < 0$ indicating flux towards the left bath, even if its temperature is higher than that of the right bath *i.e.* $T_L > T_R$ (see Fig. 4.8a). In fact, the higher is T_L, the larger is the magnitude of the heat flux $|J_L|$ towards the left bath. A similar anomalous heat transport is observed for the right flux J_R, *i.e.* the flux measured closer to the attenuating oscillator n_-. This is illustrated in Fig. 4.8b where it is shown that higher $T_R (> T_L)$ values, lead to larger heat fluxes J_R.

Our numerical experiments (see for example Fig. 4.8), indicate that γ_τ^* may often lie very close to γ_i. We can use a further analytical approximation to get a general estimation of γ_τ^* together with the scaling behavior of the currents in terms of the small-parameter $\delta\gamma = \gamma_i - \gamma$. We first note that the solution of the Lyapunov equation can be formally written in terms of a linear problem for the super-operator $\hat{S}$ acting on the matrix

space of $2N \times 2N$ matrices $\mathbf{X}$, as $\hat{\mathcal{S}}\mathbf{X} = \mathbf{Z}X + X\mathbf{Z}^T$. Specifically $\hat{\mathcal{S}}\mathbf{C}^\infty = -\mathbf{Y}$ or $\mathbf{C} = -\hat{\mathcal{S}}^{-1}\mathbf{Y} = -\sum_\tau T_\tau \hat{\mathcal{S}}^{-1}\mathbf{Y}^\tau$. Next, we define the two sets of matrices $\mathbf{V}_{\alpha,\beta} = \vec{v}_\alpha \otimes \vec{v}_\beta$, and $\mathbf{V}'_{\alpha,\beta} = \vec{v}'_\alpha \otimes \vec{v}'_\beta$, which are bi-orthonormal with respect to a matrix dot-product $(\mathbf{A},\mathbf{B}) = \mathrm{tr}\mathbf{A}^T\mathbf{B}$, *i.e.* $(\mathbf{V}_{\alpha',\beta'}, /\mathbf{V}_{\alpha,\beta}) = \delta_{\alpha,\alpha'}\delta_{\beta,\beta'}$. The latter identity can be easily derived with the help of Eq. (4.6). Using the above relations we find the spectral decomposition for the super-operator $\hat{\mathcal{S}}$ which reads as $\hat{\mathcal{S}}\mathbf{V}_{\alpha,\beta} = (\lambda_\alpha + \lambda_\beta)\mathbf{V}_{\alpha,\beta}$. This relation, together with the bi-orthonormality, allows us to derive a Liouvillean decomposition of the covariances

$$\mathbf{C}^\tau = -\sum_{\alpha,\beta} \frac{\vec{v}'_\alpha \cdot \mathbf{Y}^\tau \vec{v}'_\beta}{\lambda_\alpha + \lambda_\beta} \mathbf{V}_{\alpha,\beta}. \tag{4.16}$$

Eq. (4.16) is a very useful approximation in the vicinity of γ_i, (*i.e.* for small $\delta\gamma$) since then, in our case (See Fig.2), only a single pair of eigenvalues $\lambda_{1,2}$ dominates. Writing $\lambda_{1,2} \approx -\rho\,\delta\gamma \pm \mathrm{i}\Omega$ where $\rho = -\partial\Re\lambda_{1,2}/\partial\gamma|\gamma_i$, we have

$$\mathbf{C}^\tau = (\rho\,\delta\gamma)^{-1}(\vec{v}'_1 \cdot \mathbf{Y}^\tau \vec{v}'_2)(\mathbf{V}_{1,2} + \mathbf{V}_{2,1})/2 + \mathcal{O}((\delta\gamma)^0) \tag{4.17}$$

Eq. (4.17) together with Eq. (4.7) yields an approximate expression of the current J_n near γ_i

$$J_\tau = (1/\delta\gamma)(\mathcal{K}^\tau_L T_L + \mathcal{K}^\tau_R T_R) + \mathcal{O}((\delta\gamma)^0) \tag{4.18}$$

where $\mathcal{K}^\tau_{\tau'}$ are γ and temperature independent coefficients. The divergence $J_\tau \sim 1/\delta\gamma$ is nicely seen in Fig. 4.8.

To strengthen further the validity of our approximations for the covariant matrix Eq. (4.17) we have calculated the temperature profile $T_n \equiv \langle p_n^2 \rangle = C_{N+n,N+n}$ and the current profile defined by Eq. (4.7). In Fig. 4.9 we compare the outcome of Eq. (4.5) with the predictions of Eq. (4.17) and find an excellent agreement as $\delta\gamma \to 0$.

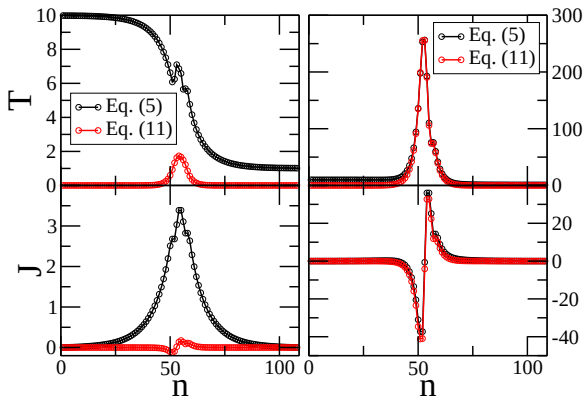

Figure 4.9: Flux and temperature profiles for two different situations of a chain with $N_a = 8$ and $N_b = 50$ sites. The bath temperatures are $T_L = 10$, $T_R = 1$ while the coupling to the bath is $\kappa = 0.1$: left plots correspond to $\gamma = 0.1$, far away from the critical value $\gamma_i = 0.289$, while the right plots are for $\gamma = 0.286$ much closer to γ_i. The black curves correspond to exact solution of Eq. (4.5), while the red curves are associated with the analytical approximation Eq. (4.17).

4.3 Electronic Implementation

Theoretical work needs to be experimentally tested and thus, we propose an LRC circuit capable of demonstrating the qualitative features of the active harmonic lattice [10]. The proposed experiment is shown in Fig. 4.10. The heat baths are implemented by synthesized noise sources V_n and V_n' having spectral density functions $S(\omega) = \frac{2}{\pi} k_B T r \sqrt{1 - \omega^2 LC/4}$, with a fixed series resistance $r = \sqrt{L/C}$, and T the respective bath temperature. This spectral density along with the $L/2$ coupling into the ends of the system closely matches the Langevin reservoir of our lattice model. Moreover, the linear nature of the system allows for a computational correction of both the spectral function and impedance of the experimental bath to the infinite chain equivalent. The gain is implemented by a negative impedance converter [47] configured as a negative resistance. The lattice chain has an exact electronic equivalence to an LC chain with the gain (loss) taken as a series negative resistance (resistance). The in-

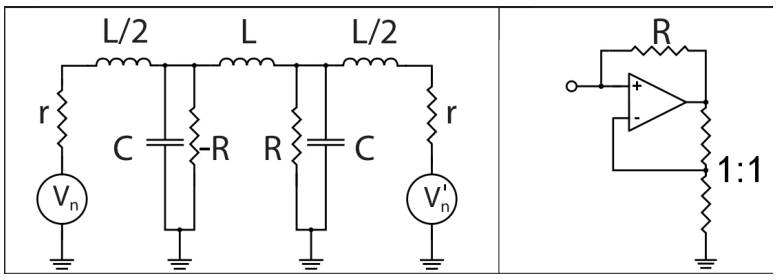

Figure 4.10: Electronic implementation of a simplified $N_a = 2$ (dimer) chain. The negative resistance gain element is provided by the op-amp negative impedance converter shown in left. The voltage sources V_n and V_n' are synthesized noise generators which, along with the fixed r stand in for the thermal baths.

herent instability of a negative resistance discrete element LR combination precludes, however, this direct implementation. The gain and loss in the electronic dimer version are introduced as a parallel resistance elements. The net power conducted out of either bath can be obtained from the voltages sampled on the respective source resistance. For example, if $V(t)$ is the voltage on the upper end of the left bath resistance r (see Fig 4.10), the power conducted out of that bath is $W_n = \langle V(t)(V_n(t) - V(t))\rangle/r$. A negative power would indicate heat flux into the bath.

4.4 Summary

We have demonstrated that heat transport in $\mathcal{PT}$-symmetric harmonic chains can exhibit unique characteristics. The non-equilibrium steady state solution was found and studied in detail. We have found that the heat flux has negative differential thermal conductance, it is independent of the temperature of the bath that is on the other end of the chain, and shows a non-reciprocal behavior with respect to the two baths. Lastly, an electronic implementation where our theory can be test was proposed.

Chapter 5

Conclusion

The importance of symmetries in transport phenomena has been studied and recognized in a variety of frameworks ranging from electronics, to optics, molecular physics, bio-physics and energy transport in biological systems. Examples of such fundamental symmetries that we often find in nature are parity and time-reversal symmetries. Recently, there has been considerable research interest in systems that do not obey the parity and time-reversal symmetries separately, but respect the combined parity and time-reversal symmetry. These systems exhibit real spectra despite the fact that they are in general non-Hermitian due to the presence of various gain/loss mechanisms. The ability to realize such types of systems in the optics framework generates further theoretical interest in understanding their properties. Among the theoretical predictions are power oscillations, loss induced optical transparency, double refraction, and nonreciprocal beam dynamics.

In this thesis, we investigated to what extent such novel features are present in the framework of heat transport by using a simple $\mathcal{PT}$-symmetric harmonic model coupled to Langevin heat reservoirs. We study the non-equilibrium steady-state properties of this system, such as the temperature profile and flux, by employing the Liouvillian approach and Ito calculus of stochastic differential equations. Our main result reveals a

heat flux that can have a negative differential thermal conductance and can be independent of the temperature of the reservoir on the other end of the chain. Moreover, the heat flux shows a nonreciprocal behavior with respect to the two baths. Finally, we propose an electronic experimental set-up where our predictions can be tested.

Obviously, our current study only scratches the surface of $\mathcal{PT}$-thermal transport. Many questions still remain to be answered. For example, it is not obvious how the interplay of nonlinearity with $\mathcal{PT}$-symmetry will affect the heat flow. Equally exciting is the investigation of the scaling behavior of the thermal conductance with the system size. The main question here is to what extent the Fourier law will affected by the nonreciprocal heat flow in $\mathcal{PT}$-symmetric systems. The answers to these questions will not only enhance our fundamental understanding of $\mathcal{PT}$-symmetry, but it might also lead to new proposals for the creation of novel thermal devices and the design of efficient schemes for the control of heat transport.

Appendix A

Eigenvalues in the Broken $\mathcal{PT}$ Phase

A $\mathcal{PT}$-symmetric Hamiltonian has to satisfy the following commutation relation:

$$[\mathcal{PT}, H] = 0 \tag{A.1}$$

Let us define the eigenvectors and eigenvalues of H as $H|\psi\rangle = E|\psi\rangle$. Then, the commutation relation implies

$$\begin{aligned} H\mathcal{PT}|\psi\rangle &= \mathcal{PT}H|\psi\rangle \\ H\mathcal{PT}|\psi\rangle &= \mathcal{PT}E|\psi\rangle \end{aligned} \tag{A.2}$$

Since, $\mathcal{PT}$ is an anti-linear operator, we get:

$$H\mathcal{PT}|\psi\rangle = E^*\mathcal{PT}|\psi\rangle \tag{A.3}$$

This tells us that $|\psi\rangle$ and $\mathcal{PT}|\psi\rangle$ are both eigenvectors of the Hamiltonian H. Also, both E and E^* are eigenvalues of H. In the exact $\mathcal{PT}$-symmetric phase where H and $\mathcal{PT}$ share the same set of eigenvectors, the eigenvalues have to be strictly real because

$E = E^*$. In the broken $\mathcal{PT}$-symmetric case where $\mathcal{PT}$ and H no longer share the same eigenvectors, the eigenvalues of H comes in complex conjugate pairs.

Appendix B

Left and Right Eigenvectors

Recall that for the $\mathcal{PT}$-symmetric Hamiltonian, we have the following left and right eigenvectors:

$$\langle L_n|H = \langle L_n|E_n; \qquad H|R_n\rangle = E_n|R_n\rangle \tag{B.1}$$

Let us focus on the left eigenvectors first and take its transpose:

$$\begin{aligned} (\langle L_n|H)^T &= (\langle L_n|E_n)^T \\ H^T|L_n\rangle &= E_n|L_n\rangle \end{aligned} \tag{B.2}$$

For a $\mathcal{PT}$-symmetric Hamiltonian, $H = H^T$, therefore, we get

$$H|L_n\rangle = E_n|L_n\rangle \tag{B.3}$$

Since this has to be equivalent to the right eigenvectors, we can conclude that the left (right) eigenvectors is the transpose of the corresponding right (left) eigenvectors

$$(\langle L_n|)^T = |R_n\rangle. \tag{B.4}$$

Appendix C

A Rigorous Definition of Temperature

A rigorous definition of temperature starts with the entropy S. In the micro-canonical ensemble, entropy plays the role of a generalized thermodynamic potential which determines other thermodynamic observables.

Specifically, temperature can be defined from the well known thermodynamic relation:

$$\frac{1}{T} = \left(\frac{\partial S}{\partial E}\right)_V \tag{C.1}$$

where V indicates taking the partial derivative keeping the volume fixed. So what is

the entropy for the micro-canonical ensemble? There are two choices [48]:

$$\begin{aligned}
(A) \qquad S(E,N,V) &= \ln(c_N\omega(E,N,V)) = \ln\left(c_N\int dqdp\delta(E-H(q,p))\right) \\
&= \ln\left(c_N\int_{H=E}\frac{d\sigma}{\|\bigtriangledown H\|}\right) \\
(B) \qquad S(E,N,V) &= \ln(c'_N\Omega(E,N,V)) = \ln\left(c'_N\int dqdp\Theta(E-H(q,p))\right) \\
&= \ln\left(c'_N\int_{H\leq E}d\Gamma\right) \qquad \text{(C.2)}
\end{aligned}$$

In both of these choices, the Boltzmann constant, $k_B = 1$, and c_N and c'_N are arbitrary constants that makes the argument in the logarithm dimensionless. q and p are the generalized position and momentum coordinates.

Definition (A) includes all of the microstates compatible with the constant $H = E$, i.e., those microstates belonging to the constant energy surface $\Sigma_E = (q,p) \in \Gamma | H(q,p) = E$. One the other hand, (B) considers those microstates contained inside the hypervolume $V_E = (q,p) \in \Gamma | H(q,p) \leq E$ limited by Σ_E. Both definitions become equivalent in the thermodynamic limit. In the following discussion, we will use (A) to arrive at our definition of temperature:

$$\frac{1}{T_\mu} = \frac{\partial S}{\partial E} = \frac{\frac{\partial\omega}{\partial E}}{\omega} \qquad \text{(C.3)}$$

Making use of a theorem of differential geometry and choosing a vector $\mathbf{u}$ such that $\bigtriangledown \cdot u = 1$, one obtains:

$$\frac{1}{T_\mu} = \frac{\int_{H=E} d\sigma/\|\bigtriangledown H\|}{\int_{H<E}\bigtriangledown\cdot\mathbf{u}d\Gamma} = \frac{\int_{H=E} d\sigma/\|\bigtriangledown H\|}{\int_{H=E}\bigtriangledown H\cdot\mathbf{u}d\sigma/\|\bigtriangledown H\|} \qquad \text{(C.4)}$$

This approach yields the same result as in Eq. (3.6).

Appendix D

Nosè-Hoover Thermostat

This appendix applies the extended system method via a virtual variable formulation to obtain the equilibrium distribution function. This derivation is taken from Ref. [42].

In the extended system (ES) method, an additional degree of freedom s is introduced and acts as an external system on the physical system of N particles, with coordinates $\mathbf{q}'_i$, masses m_i and potential energy $\phi(\mathbf{q}')$. Virtual variables (coordinate $\mathbf{q}_i$, momentum $\mathbf{p}_i$, and time t) were also introduced and they relate to the real variables ($\mathbf{q}'_i$,$\mathbf{p}'_i$, t') by

$$\begin{aligned} \mathbf{q}'_i &= \mathbf{q}_i, \\ \mathbf{p}'_i &= \mathbf{p}_i/s, \\ t' &= \int^t \frac{dt}{s} \end{aligned} \tag{D.1}$$

The real velocity ($d\mathbf{q}'_i/dt'_i$) is also expressed by a scaled form in the virtual variable formulation

$$\frac{d\mathbf{q}'_i}{dt'} = s\frac{d\mathbf{q}'_i}{dt} = s\frac{d\mathbf{q}_i}{dt} \tag{D.2}$$

Therefore, one can interpret these transformation by a time scaling $dt' = dt/s$.

The Hamiltonian of the extended system of the particles and the variable s in terms of the virtual variables is postulated as

$$H = \sum_i \mathbf{p}_i^2/2m_i s^2 + \phi(\mathbf{q}) + p_s^2/2Q + gk_BT \ln s, \tag{D.3}$$

where p_s is the conjugate momentum of s, Q is a parameter of dimension energy$\cdot$(time)^2 and behaves as a mass for the emotion of s, k_B is the Boltzmann's constant, T is the externally set temperature, the parameter g is essentially equal to the number of degrees of freedom of the physical system.

Next, Nosé assumes that the Hamiltonian formalism can be applied to Eq. D.3 with the virtual variables. The equations of motion are

$$\begin{aligned}
\frac{d\mathbf{q}_i}{dt} &= \frac{\partial H}{\partial \mathbf{p}_i} = \frac{\mathbf{p}_i}{m_i s^2}, \\
\frac{d\mathbf{p}_i}{dt} &= -\frac{\partial H}{\partial \mathbf{q}_i} = -\frac{\partial \phi}{\partial \mathbf{q}_i}, \\
\frac{ds}{dt} &= \frac{\partial H}{\partial p_s} = p_s/Q, \\
\frac{dp_s}{dt} &= -\frac{\partial H}{\partial s} = \left(\sum_i \mathbf{p}_i^2/m_i s^2 - gk_BT \right)/s.
\end{aligned} \tag{D.4}$$

In Lagrangian form, these are

$$\frac{d}{dt}\left(m_i s^2 \frac{d\mathbf{q}_i}{dt} \right) = -\frac{\partial \phi}{\partial \mathbf{q}_i} \tag{D.5}$$

or

$$\frac{d^2\mathbf{q}_i}{dt^2} = -\frac{1}{m_i s^2}\frac{\partial \phi}{\partial \mathbf{q}_i} - \frac{2}{s}\frac{ds}{dt}\frac{d\mathbf{q}_i}{dt} \tag{D.6}$$

and

$$\frac{d}{dt}\left(Q\frac{ds}{dt} \right) = \left[\sum_i s^2 \left(\frac{d\mathbf{q}_i}{dt} \right)^2 /m_i - gk_BT \right]/s. \tag{D.7}$$

The conserved quantities are the Hamiltonian H, the total momentum $\sum_i \mathbf{p}_i$, and the angular momentum $sum_i \mathbf{q}_i \times \mathbf{p}_i$.

$$\frac{dH}{dt} = \sum_i \left(\frac{\partial H}{\partial \mathbf{p}_i}\frac{d\mathbf{p}_i}{dt} + \frac{\partial H}{\partial \mathbf{q}_i}\frac{d\mathbf{q}_i}{dt} \right) + \frac{\partial H}{\partial p_s}\frac{dp_s}{dt} + \frac{\partial H}{\partial s}\frac{ds}{dt} = 0. \tag{D.8}$$

The conservation laws for the last two quantities are derived from Eq. (D.4) and the properties satisfied by the potential

$$\sum_i \frac{\partial \phi}{\partial \mathbf{q}_i} = 0 \tag{D.9}$$

and

$$\sum_i \mathbf{q}_i \times \frac{\partial \phi}{\partial \mathbf{q}_i} = 0. \tag{D.10}$$

It should be noted that during the ordinary type of simulations with periodic boundary condition, the angular momentum is not conserved.

In this case where the momentum and angular momentum is conserved, we can write down the partition function Z for N identical particles by integrating the equilibrium distribution function $\rho(x_1, x_2, \ldots)$ over the whole phase space.

$$Z = \frac{1}{N! h^{3N}} \int dx_1 \int dx_2 \ldots \rho(x_1, x_2, \ldots), \tag{D.11}$$

where h is Planck's constant and x_i is a generalized coordinate (the constant factors for ρ and Z are ignored hereafter). The projection of the equilibrium distribution function from the space (x_1, x_2) onto the space (x_1) is carried out by integrating with respect to the variable x_2,

$$\rho(x_1) = \int dx_2 \rho(x1, x2). \tag{D.12}$$

In particular, a distribution function $\rho(\mathbf{p}', \mathbf{q}')$ that is projected from the extended system onto the physical system is need. Since the total Hamiltonian, Eq. (D.3), is conserved in the extended system, this method produces a μ-canonical ensemble. The distribution function $\rho(\mathbf{p}, \mathbf{q}, p_s, s)$ is expressed as a Dirac delta function, $\delta(H - E)$. The shortened forms $d\mathbf{p} = d\mathbf{p}_1 d\mathbf{p}_2 \ldots d\mathbf{q}_N, d\mathbf{q} = d\mathbf{q}_1 d\mathbf{q}_2 \ldots d\mathbf{q}_N$, and $H_0(\mathbf{p}, \mathbf{q}) = \sum_i \mathbf{p}_i^2 / 2m_i + \phi(\mathbf{q})$ are used. The partition becomes

$$Z = \int dp_s \int ds \int d\mathbf{p} \int d\mathbf{q} \delta \left[H_0(\mathbf{p}/2, \mathbf{q}) + p_s^2/2Q + g k_b T \ln s - E \right]. \tag{D.13}$$

The virtual momenta $\mathbf{p}_i$ and coordinates $\mathbf{q}_i$ are transformed to the real variables $\mathbf{p}'_i = \mathbf{p}_i/s$, $\mathbf{q}'_i = q_i$. The volume element is $d\mathbf{p}d\mathbf{q} = s^{3N}d\mathbf{p}'d\mathbf{q}'$. Hence,

$$Z = \int dp_s \int d\mathbf{p}' \int d\mathbf{q}' \int ds \cdot s^{3N} \delta \left[H_0(\mathbf{p}', \mathbf{q}') + p_s^2/2Q + gk_BT \ln s - E \right]. \quad \text{(D.14)}$$

Because the argument of the δ function in the above equation has only one zero as a function of the variable. s, we can use the equivalence relation $\delta\left[f(s)\right] = \delta(s-s_0)/f'(s_0)$, where s_0 is the zero of $f(s)$.

$$\begin{aligned} Z &= \frac{1}{gk_BT} \int dp_s \int d\mathbf{p}' \int d\mathbf{q}' \int ds \cdot s^{3N+1} \delta(s - exp\{- \left[H_0(\mathbf{p}', \mathbf{q}') + p_s/2Q - E \right] / gk_BT\}) \\ &= \frac{1}{gk_BT} \exp\left[\left(\frac{3N+1}{g} \right) E/k_BT \right] \int dp_s \exp\left[- \left(\frac{3N+1}{g} \right) p_s^2/2Qk_BT \right] \\ &\int d\mathbf{p}' \int d\mathbf{q}' \exp\left[- \left(\frac{3N+1}{g} \right) H_0(\mathbf{p}', \mathbf{q}')/k_BT \right]. \end{aligned} \quad \text{(D.15)}$$

Upon choosing $g = 3N+1$, the partition function of the extended system is equivalent to that of the physical system in the canonical ensemble except for a constant factor:

$$Z = C \int d\mathbf{p}' \int d\mathbf{q}' \exp\left[-H_0(\mathbf{p}', \mathbf{q}')/k_BT \right]. \quad \text{(D.16)}$$

Appendix E

Algebra for the correlation function

$$
\begin{aligned}
C_v(t_2 - t_1) &= \langle (v(t_2) - \langle v(t_2) \rangle) \cdot (v(t_1) - \langle v(t_1) \rangle) \rangle_\xi \\
&= \langle \int_0^{t_2} ds e^{-\lambda(t_2 - s)} f(s) \cdot \int_0^{t_1} ds e^{-\lambda(t_1 - s)} f(s) \rangle_\xi \\
&= \int_0^{t_2} \int_0^{t_1} ds_1 ds_2 e^{-\lambda(t_1 + t_2 - s_1 - s_2)} \langle f(s_1) f(s_2) \rangle_\xi \\
&= \int_0^{t_2} \int_0^{t_1} ds_1 ds_2 e^{-\lambda(t_1 + t_2 - s_1 - s_2)} \sigma^2 \delta(s_1 - s_2) \\
&= \sigma^2 \int_0^{t=\min(t_1, t_2)} ds_2 e^{-\lambda(t_1 + t_2 - 2s_2)} \\
&= \frac{\sigma^2}{2\lambda} e^{-\lambda(t_1 + t_2)} \int_0^t dy e^y \\
&= \frac{\sigma^2}{2\lambda} (e^{2\lambda t} - 1) \\
&= \frac{\sigma^2}{2\lambda} \{ e^{-\lambda(t_1 + t_2 - 2t)} - e^{-\lambda(t_1 + t_2)} \}
\end{aligned} \tag{E.1}
$$

Finally, noting that whether $t = t_1$ or $t = t_2$, the difference of t_1 and t_2 is positive.

Therefore, we arrived at

$$C_v = \frac{\sigma^2}{2\lambda}\{e^{-\lambda|t_1-t_2|} - e^{-\lambda(t_1+t_2)}\} \tag{E.2}$$

Appendix F

Implementing Ito Calculus

As shown in the previous appendix that the Langevin equation can be written in the following form

$$d\vec{x} = \mathbf{Z}\vec{x}dt + \mathbf{D}d\vec{\xi} \tag{F.1}$$

where $\mathbf{D}$ is a diagonal matrix and

$$\vec{x} = \begin{pmatrix} \vec{q} \\ \vec{p} \end{pmatrix} \tag{F.2}$$

In order to solve this stochastic differential equation, we define a matrix by taking the tensor product of $\vec{x}$

$$\mathbf{C} = \langle \vec{x} \otimes \vec{x} \rangle \tag{F.3}$$

We proceed by taking the derivative of the product of the vector components:

$$\begin{aligned} d(x_i x_j) &= (x_i + dx_i)(x_j + dx_j) - x_i x_j \\ &= x_i dx_j + (dx_i)x_j + dx_i dx_j \\ &= x_i \sum_k Z_{jk} x_k dt + x_i D_j d\xi_j + (\sum_k Z_{ik} x_k) x_j dt + x_j D_i d\xi_i + D_i D_j d\xi_i d\xi_j \end{aligned} \tag{F.4}$$

Taking an average of Eq. (F.4) and using the property $\langle d\xi_i d\xi_j \rangle = \delta_{ij} dt$, Eq.(F.4) simplifies to

$$\frac{d\langle x_i x_j \rangle}{dt} = \sum_k Z_{jk} \langle x_i x_k \rangle + \sum_k Z_{ik} \langle x_k x_j \rangle + \delta_{ij} D_i^2 \tag{F.5}$$

Since $C_{ij} = \langle x_i x_j \rangle$, the above equation yields:

$$\frac{d\mathbf{C}}{dt} = \mathbf{C}\mathbf{Z}^T + \mathbf{Z}\mathbf{C} + \mathbf{Y} \tag{F.6}$$

in which $Y_{ij} = D_i^2 \delta_{ij}$.

Appendix G

Fokker-Planck Equation

Recall that the Langevin equation takes the following form:

$$\frac{dx}{dt} = -\gamma x + b\xi(t) \tag{G.1}$$

where b are both functions of x and t. The physical meaning of γ and b will become clear at the of this derivation.

Let us consider an arbitrary function $x(t)$:$f[x(t)]$. We would like to know what stochastic differential equation it obeys. We start by considering a general function $f[x(t)]$, whose derivative can be written as

$$\begin{aligned} df[x(t)] &= f[x(t) + dx(t)] - f[x(t)] \\ &= f[x(t)] + f'[x(t)]dx + \frac{1}{2}f''[x(t)](dx)^2 - f[x(t)] + \cdots \\ &= f'[x(t)]\{-\gamma x dt + b\xi(t)dt\} + \frac{1}{2}f''[x(t)]\{-\gamma x dt + b\xi(t)dt\}^2 + \cdots \end{aligned} \tag{G.2}$$

By definition, $\xi(t)dt = dW(t)$, where $dW(t)$ denotes the wiener process. Therefore, we

obtain

$$\begin{aligned} df[x(t)] &= f'[x(t)]\{-\gamma x dt + b dW(t)\} + \frac{1}{2} f''[x]\{\gamma^2 x^2 dt^2 + b^2 dW(t)^2 - 2\gamma x b dW(t) dt\} \\ &= f'[x(t)]\{-\gamma x dt + b dW(t)\} + \frac{1}{2} f''[x(t)] b^2 dW(t)^2 \\ &= \{-\gamma x f'[x(t)] + \frac{1}{2} b^2 f''[x(t)]\} dt + b f'[x(t)] dW(t). \end{aligned} \tag{G.3}$$

In the above equation, we have used the definition $dW(t)^2 = dt$, $dt^2 = 0$ and $dW(t)dt = 0$. The time development of $f[x(t)]$ is simply

$$\begin{aligned} \frac{\langle df[x(t)]\rangle}{dt} &= \langle \frac{df[x(t)]}{dt} \rangle = \frac{d}{dt} \langle f[x(t)]\rangle \\ &= \langle -\gamma x f'[x(t)] + \frac{1}{2} b^2 f''[x(t)]\rangle \end{aligned} \tag{G.4}$$

Now, taking into consideration that $x(t)$ follows a distribution $\rho[x(t)]$, the above equation becomes

$$\begin{aligned} \frac{d}{dt}\langle f[x(t)]\rangle &= \frac{d}{dt} \int \rho[x(t)] f[x(t)] dx = \int dx f[x(t)] \frac{d}{dt} \rho[x(t)] \\ \langle -\gamma x f'[x(t)] + \frac{1}{2} b^2 f''[x(t)]\rangle &= \int dx \{-\gamma x f'[x(t)] + \frac{1}{2} b^2 f''[x(t)]\} \rho[x(t)] \\ &= \int \frac{d}{dt} \rho[x(t)] f[x(t)] dx \end{aligned} \tag{G.5}$$

Integrating by parts and ignoring surface terms, we obtain:

$$\frac{\partial}{\partial t} \rho[x(t)] = \gamma \frac{\partial}{\partial x} [x(t) \rho[x(t)]] + \frac{1}{2} \frac{\partial^2}{\partial x^2} [b^2 \rho[x(t)]] \tag{G.6}$$

Eq. (G.6) is known as the Fokker-Planck Equation. It captures the diffusion process defined by a drift coefficient γ and a diffusion coefficient b^2.

Bibliography

[1] S. Lepri, R. Livi, and A. Politi. Thermal conduction in classical low-dimensional lattices. *Phys. Rep.*, 377:1, 2003.

[2] F. Bonetto, J. L. Lebowitz, and L. Rey-Bellet. *Mathematical Physics 200*. Imperial College London, 2000.

[3] A. Dhar. Heat transport in low-dimensional systems advances in physics. *Adv. Phys.*, 57:457, 2008.

[4] M. Terraneo, M. Peyrard, and G. Casati. Controlling the energy flow in nonlinear lattices: A model for a thermal rectifier. *Phys. Rev. Lett.*, 88:094392, 2002.

[5] B. Li, L. Wang, and G. Casati. Thermal diode: Rectification of heat flux. *Phys. Rev. Lett.*, 93:184301, 2004.

[6] L. Wang and B. Li. Thermal logic gates: Computation with phonons. *Phys. Rev. Lett.*, 99:177208, 2007.

[7] C. W. Chang, D. Okawa, A. Majumdar, and A. Zettl. Solid-state thermal rectifier. *Science*, 314:1121, 2006.

[8] W. Kobayashi, Y. Teraoka, and I. Terasaki. An oxide thermal rectifier. *Appl. Phys. Lett.*, 95:171905, 2009.

[9] T. Prosen and D. K. Campbell. Normal and anomalous heat transport in one-dimensional classical lattices. *Chaos*, 15:015117, 2005.

[10] M. C. Zheng, F. Ellis, R. Fleischmann, T. Prosen, T. Kottos, and T. Geisel. Heat transport in pt-symmetric harmonic chains. *Submitted*, 2011.

[11] K. G. Makris, R. El-Ganainy, D. N. Christodoulides, and Z. H. Musslimani. Beam dynamics in PT symmetric optical lattices. *Phys. Rev. Lett.*, 100(10):103904, Mar 2008.

[12] Tsampikos Kottos. Optical physics: Broken symmetry makes light work. *Nature Physics*, 6(166), 2010.

[13] Konstantinos G. Makris Ramy El-Ganainy Demetrios N. Christodoulides Mordechai Segev Christian E. Rüter and Detlef Kip. Observation of parity–time symmetry in optics. *Nature Physics*, 6(192), 2010.

[14] H. Ramezani, T. Kottos, R. El-Ganainy, and D. N. Christodoulides. Unidirectional nonlinear pt-symmetric optical structures. *Phys. Rev. A*, 82(043803), 2010.

[15] C. M. Bender. Making sense of non-hermitian hamiltonians. *Rep. Prog. Phys.*, 70(947), 2007.

[16] S. Boettcher C. M. Bender and P. N. Meisinger. PT-symmetric quantum mechanic. *J. Math. Phys.*, 40(2201), 1999.

[17] Ali Mostafazadeh. Spectral singularities of complex scattering potentials and infinite reflection and transmission coefficients at real energies. *Phys. Rev. Lett.*, 102(22):220402, Jun 2009.

[18] Carl T. West, Tsampikos Kottos, and Tomaž Prosen. PT-symmetric wave chaos. *Phys. Rev. Lett.*, 104(5):054102, Feb 2010.

[19] Oliver Bendix, Ragnar Fleischmann, Tsampikos Kottos, and Boris Shapiro. Exponentially fragile PT symmetry in lattices with localized eigenmodes. *Phys. Rev. Lett.*, 103(3):030402, Jul 2009.

[20] Shachar Klaiman, Uwe Günther, and Nimrod Moiseyev. Visualization of branch points in PT-symmetric waveguides. *Phys. Rev. Lett.*, 101(8):080402, Aug 2008.

[21] S. Longhi. Bloch oscillations in complex crystals with PT symmetry. *Phys. Rev. Lett.*, 103(12):123601, Sep 2009.

[22] Z. H. Musslimani, K. G. Makris, R. El-Ganainy, and D. N. Christodoulides. Optical solitons in PT periodic potentials. *Phys. Rev. Lett.*, 100(3):030402, Jan 2008.

[23] M. C. Zheng. Non-hermitian dynamics: Examples from disordered microwave cavities and classical optics. WesScholar, April 2010.

[24] Carl M. Bender, Dorje C. Brody, Hugh F. Jones, and Bernhard K. Meister. Faster than hermitian quantum mechanics. *Phys. Rev. Lett.*, 98(4):040403, Jan 2007.

[25] A. Guo, G. J. Salamo, D. Duchesne, R. Morandotti, M. Volatier-Ravat, V. Aimez, G. A. Siviloglou, and D. N. Christodoulides. Observation of PT-symmetry breaking in complex optical potentials. *Phys. Rev. Lett.*, 103(9):093902, Aug 2009.

[26] Z. Lin, H. Ramezani, T. Eichelkraut, T. Kottos, H. Cao, and D. N. Christodoulides. Unidirectional invisibility induced by pt-symmetric periodic structures. *Submitted*, 2011.

[27] S. Jensen. The nonlinear coherent coupler. *IEEE Quantum Electronics*, 18:1580, 1982.

[28] V. M. Kenkre and D. K. Campbell. Self-trapping on a dimer: Time-dependent solutions of a discrete nonlinear schrödinger equation. *Phys. Rev. B*, 34:4959.

[29] B. E. A. Saleh and M. C. Teich. *Fundamentals of Photonics*. Wiley, New York, 1991.

[30] R. Philip, M. Anija, C. S. Yelleswarapu, and D. V. G. L. N. Rao. Passive all-optical diode using asymmetric nonlinear absorption. *Appl. Phys. Lett.*, 91(141118), 2007.

[31] K. Gallo, G. Assanto, K. R. Parameswaran, and M. M. Fejer. All-optical diode in a periodically poled lithium niobate waveguide. *Appl. Phys. Lett.*, 79:1386407, 2001.

[32] K. Gallo and G. Assanto. All-optical diode based on second-harmonic generation in an asymmetric waveguide. *J. Opt. Soc. Am. B*, 16:267, 1999.

[33] M. Scalora, J. P. Dowling, C. M. Bowden, and M. J. Bloemer. The photonic band edge optical diode. *J. Appl. Phys.*, 76:2023, 1994.

[34] F. Biancalana. All-optical diode action with quasiperiodic photonic crystals. *J. Appl. Phys.*, 104:093113, 2008.

[35] H. Zhou, K.-F. Zhou, W. Hu, Q. Guo, S. Lan, X.-S. Lin, and A. V. Gopal. All-optical diodes based on photonic crystal molecules consisting of nonlinear defect pairs. *J. Appl. Phys.*, 99:123111, 2006.

[36] C. Kittel. *Introduction to Solid State Physics*. Wiley, New York, 2005.

[37] R. D. Astumian and P. Hänggi. Brownian motors. *Phys. Today*, 55:33, 2002.

[38] F. Jülicher, A. Ajdari, and J. Prost. Modeling molecular motors. *Rev. Mod. Phys.*, 69:1269, 1997.

[39] P. Reimann. Brownian motors: noisy transport far from equilibrium. *Phys. Rep.*, 361:57, 2002.

[40] S. R. Groot and P. Mazur. *Non-Equilibrium Thermodynamics*. Dover, New York, 1984.

[41] Daan Frenkel and B. Smit. *Understanding Molecular Simulation: From Algorithms to Applications*. Academic Press, Aug 1996.

[42] S. Nóse. A unified formulation of the constant temperature molecular dynamics methods. *J. Chem. Phys.*, 81:511, 1984.

[43] C. M. Bender and S. Boettcher. Real spectra in non-hermitian hamiltonians having pt symmetry. *Phys. Rev. Lett.*, 80:5243, 1998.

[44] C. M. Bender, D. C. Brody, and H. F. Jones. Complex extension of quantum mechanics. *Phys. Rev. Lett.*, 89:270401, 2002.

[45] M. Znojil. Pt-symmetric square well. *Phys. Lett. A*, 285:7, 2001.

[46] H. F. Jones. Gauging non-hermitian hamiltonians. *J. Phys. A: Math. Theor.*, 42(13):135303, 2009.

[47] P. Horowitz and W. Hill. *The Art of Electronics*. Cambridge University Press, 2 edition, 1989.

[48] C. Giardiná and R. Livi. Ergodic properties of microcanonical oberservables. *J. Stat. Phys.*, 91:1027, 1998.